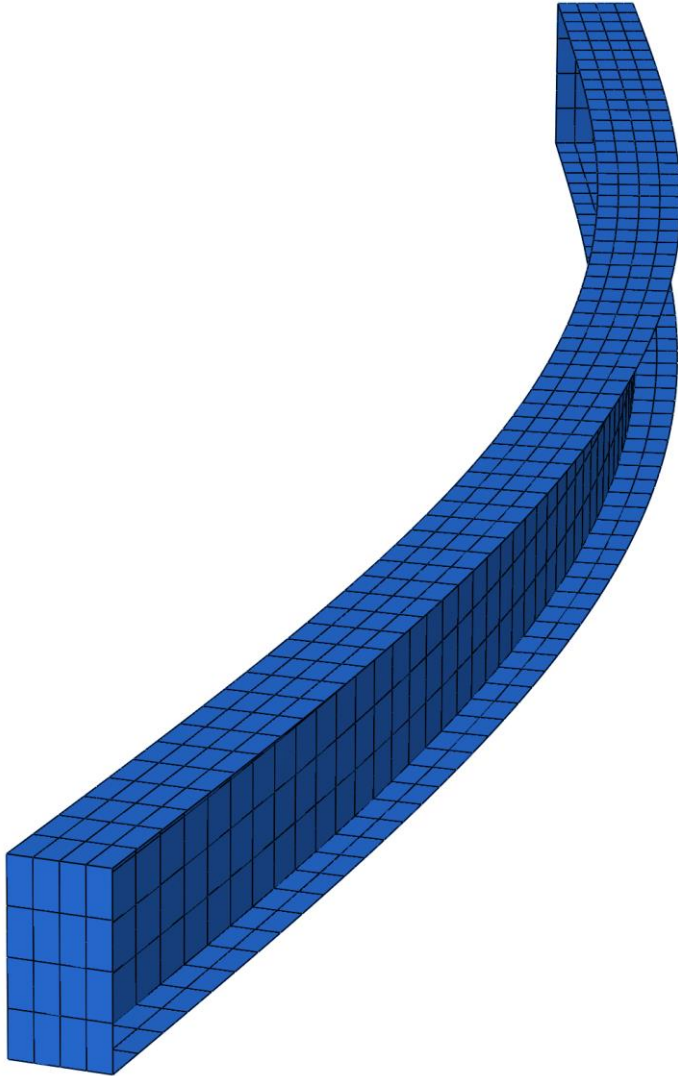


Analysis of Imperfections in Structural Columns



Master Thesis
4th Semester MSc. - Civil Engineering
Aalborg University
Spring 2014

Martin Christensen
Peter Roug

Department of Civil Engineering

Aalborg University
Sohngårdsholmsvej 57
9000 Aalborg
www.ses.aau.dk

Title:

Analysis of Imperfections in Structural Columns

Authors:

Martin Christensen
Peter Roug

Project period:

Master Thesis
01-02-2014 to 10-06-2014

Supervisors:

Henrik Stensgaard Toft
Søren Madsen

Printed editions:

5

Number of pages:

63 + CD

Abstract:

This thesis involves an analysis of the load capacity of slender IPE160 steel columns limited by global instability, by means of analytical and numerical calculations. The analytical calculations will be conducted in correspondence to the current [DS/EN-1993-1-1, 2007] standard, while the numerical analysis will be performed in the commercial software Abaqus. The calculations are limited to uniaxial compressed, simple supported columns, subjected to a variety of imperfections.

The load capacity is compared with experimental data found in literature and the model uncertainties are determined. The results obtained in the project are used to calculate reliability index and partial safety factors, by FORM which is verified through Monte Carlo Simulation. Subsequently the calculated partial safety factors are discussed and a calibration is conducted.

The column behavior is reviewed continuously throughout the project, and a history review with State-of-the-Art are reviewed in order to assess the influence on current standards.

Martin Christensen

Peter Roug

Preface

This project is made in the period: 03-02-2014 to 10-06-2014. The project theme is "*Imperfections in Structural Columns*" on the 4th semester of the Master program in *Structural and Civil Engineering* under the *School of Engineering and Science* at *Aalborg University*.

Knowledge from previous semesters and earlier projects will be used as basis of the project.

Readers Guide

Through this Master thesis, the Harvard Method is used to refer to all sources, by [Surname, year], except for references to the Standards which will be referred to as [Standard, year]. Three main sources of literature are used, namely books, articles and technical reports, which are all listed in the bibliography, located at the end of the thesis. For sources with more than a two authors, only the main author will be mentioned by name, while other contributing authors are mentioned as "et al.". Sources on figures are displayed in the caption below the figure. Figures, tables and equation are numbered, regarding to the present chapter, *i.e.* figures in *e.g.* chapter 5 is call Figure 5.1, Figure 5.2 etc.

Main Programs

For the calculations conducted through this thesis, both commercial and open source software has been used. For the numerical simulations, the commercial software Abaqus has been used. For general data processing commercial software Matlab is used, while the open source toolbox FERUM (Finite Estimation of Reliability Using Matlab) has been used for stochastic analysis.

Digital Appendix

The digital appendix will be available on the CD in the back of the report. Files on the appendix CD is divided according to the given chapter in which they are used.

Contents

1	Introduction	1
1.1	History Review and State-of-the-Art	1
1.2	Beam theory	3
1.3	Derivation of the Critical Euler Load	5
1.4	Thesis Statement	9
I	Buckling and Imperfection Study	11
2	Reference Geometry and material properties	13
2.1	Reference Geometry	13
2.2	Reference material properties	13
2.3	Column Stability Experiments	14
3	Load Capacity by DS/EN 1993-1-1	17
3.1	Imperfections	17
3.2	Partial Safety Factor	18
3.3	Design Equations	18
4	Initial Finite Element Considerations	21
4.1	Shell analysis	21
4.2	Numerical Solvers in Abaqus	24
4.3	Boundary Conditions and loads	24
4.4	Shell Element Study	26
4.5	Verification of Mesh	27
5	Imperfections in Finite Element	29
5.1	Geometrical imperfections	29
5.2	Material imperfections	34
5.3	Installation imperfections	35
5.4	Combinations	36
5.5	Data process for Stochastic chapter	39
II	Stochastic Analysis	41
6	Model Uncertainty Estimation	43
6.1	Calculation Method - DS/EN 1990, Annex D.8	43
6.2	Model uncertainty for DS/EN	44
6.3	Model uncertainty for the Finite Element Model	44
7	Stochastic Modeling	47
7.1	Stochastic Variables	47
7.2	Design Equation	48

7.3	Limit State Function	50
7.4	Reliability index	51
8	Stochastic results	53
8.1	Reliability Analysis for the Current DS/EN Partial Safety Factor	53
8.2	Sensitivity Analyses	54
8.3	Calibration of Partial Safety Factor	55
8.4	Review of Results	56
9	Conclusion	59
	Bibliography	61
A	Limit state function	

1 Introduction

A structural column is an element which, through compression, transfers the load from above lying structures to elements below, *i.e.* an element subjected to axial loading. A well known problem when working with columns is global instability, where failure will occur before the ultimate stress of the element has been met. This phenomenon occurs due to, high slenderness, *i.e.* high ratio between the height and cross sectional area of the column, which is often used in structural engineering. As global buckling is often the limiting factor of uni-axially compressed columns, it is a field of great importance, and will be reviewed through this thesis.

1.1 History Review and State-of-the-Art

The earliest examples of post buckling and elastic instability studies are dated back to [Van Musschenbroek, 1729]. By experiments he discovered proportionality between the squared length of columns and the load capacity. In 1744 Euler proved the same proportionality theoretically, [Euler & Oldfather, 1933], defined in Eq.(1.1)

$$N_{cr} = \frac{\pi^2 EI}{l_s^2} \quad (1.1)$$

N_{cr}	Critical Euler load [N]
E	Modulus of elasticity [Pa]
I	Moment of inertia [m ⁴]
l_s	Effective column length [m]

Euler's equation was generally considered to overestimate the load capacity for short columns with low slenderness ratios. Therefore, in the last decade of the 19th century, A. Considère and F. Engesser independently suggested, that the true load capacity in the inelastic range could be obtained by using the Tangent Modulus, E_T , instead of Modulus of elasticity, E , shown in Figure 1.1. From this, the expression, seen in Eq.(1.2), called *Tangent Modulus Theory*, was formulated, [Johnston, 1983].

$$N_T = \frac{\pi^2 E_T I}{l_s^2} \quad (1.2)$$

E_T	Tangent Modulus [Pa]
-------	----------------------

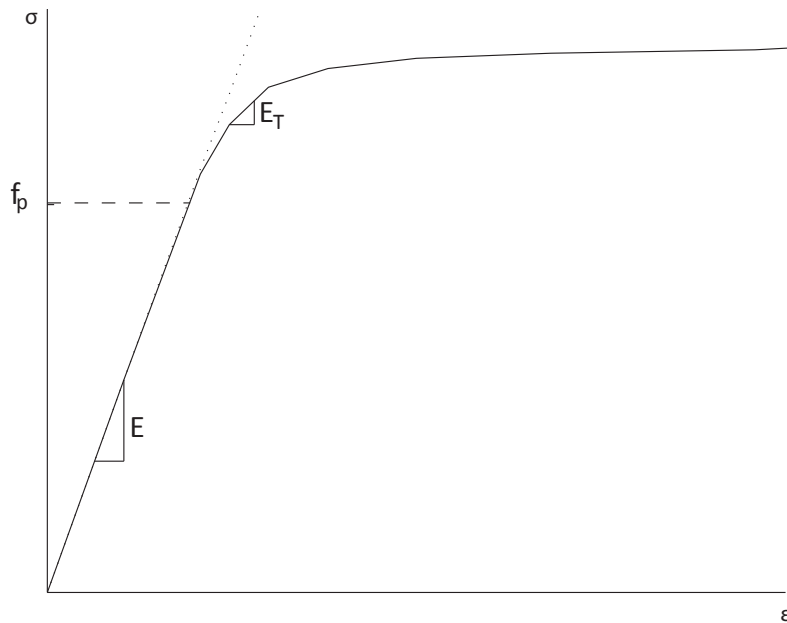


Figure 1.1. The general stress-strain relationship, f_p , indicates the point where there is no longer proportionality between the strain and stresses, *i.e.* Modulus of elasticity, E , is no longer constant and Hooke's Law becomes invalid.

In 1895 F. Engesser produced a corrected formula for a reduced modulus, not only dependent on the Tangent Modulus, but also on the cross sectional shape, Eq.(1.3), [Ziemian, 2010], named *Reduced Modulus Theory*.

$$N_r = \frac{\pi^2 E_r I}{l_s^2} \quad (1.3)$$

E_r	Reduced Modulus - $(EI_1 + E_T I_2)/I$ [Pa]
I_1	Area moment of inertia relative to the compressed portion of the cross section at the buckling state [m ⁴]
I_2	Area moment of inertia relative to the strain reversed portion of the cross section at the buckling state [m ⁴]

However, as the reduced modulus theory was considered to be correct, but proved difficult to calculate, and the tangent modulus theory was believed to underestimate the load capacity, a viable solution was yet to be discovered. Nevertheless the tangent modulus theory was relatively easy to use, and was therefore, according to [Usami & Itoh, 1998], the preferred method. Both methods were, however, used up to the first half of the 20th century for inelastic column behavior. It was later proved by [Shanley, 1947] that the tangent modulus, yielded a lower bound solution, while the reduced modulus yielded an upper bound solution. The correct column strength solution was therefore considered to be somewhere between the two bounds.

By the late 1940s more advanced tools became available, which enabled researchers to measure residual stresses within elements, perform precise full-scale experiments and run analyses using computers. In the mid-1950s the Column Research Council (CRC, later known as the Structural Stability Research Council, SSRC), formulated the CRC Column Formula, Eq.(1.4), [Ziemian, 2010],

which is still used in various standards today [Usami & Itoh, 1998].

$$N_C = \frac{\pi^2 E_T I}{K l_s^2} \quad (1.4)$$

K | Constant, varying from 0.5 to 2, depending on boundary conditions.

From the 1950s up to the 1970s, two different design methods were used: The CRC model, Eq.(1.4), which included residual stresses but ignored geometrical imperfections, and the DIN 4114 model, which included geometrical imperfections but ignored residual stresses. No models, which accounted for both phenomenon, were yet available due to the limited computational power at the time. However, by the late 1960s sufficiently powerful computational tools became available and both phenomenon could be accounted for, [Usami & Itoh, 1998].

Today, a variation of the same modified equations are in use in the DS/EN standard, seen in Eq. (1.5), and will be more thoroughly explained in Chapter 3.

$$N_{Rd} = \frac{\chi f_y A}{\gamma_{M1}} \quad (1.5)$$

N_{Rd}	Design load capacity [N]
f_y	Yield stress [MPa]
A	Cross sectional area [m ²]
γ_{M1}	Partial safety factor [—]
χ	Column reduction factor [—]

Due to the advancement of Finite Element Modeling a lot of research on how to improve the imperfection factors and how to optimize the model uncertainties are conducted presently.

According to [Papadopoulos et al., 2012] several works on stochastic imperfections were published during the last decade. [Stavrev et al., 2013] suggests, that the stochastic imperfection model should be derived by either a variation of the critical eigenmode with a random scalar variable, or through more advanced theory of random fields, which [Papadopoulos et al., 2012] furthermore suggests can be simulated as a standard numerical procedure, or by the spectral representation method.

1.2 Beam theory

A number of different methods exists for analysis of a column. Through this section, the approach best suited for capturing the bending shapes, investigated in this thesis is discussed. The different approaches which will be discussed involves Bernoulli-Euler Beam Theory and Timoshenko Beam Theory.

In 1750, Leonard Euler and Daniel Bernoulli, formulated the Bernoulli-Euler beam Theory, [Haukaas, 2012]. The theory is based on the following key assumptions:

- Material behaves linearly according to Hooke's Law.

- Plane sections remain plane and perpendicular to the neutral axis during bending, seen in Figure 1.2.

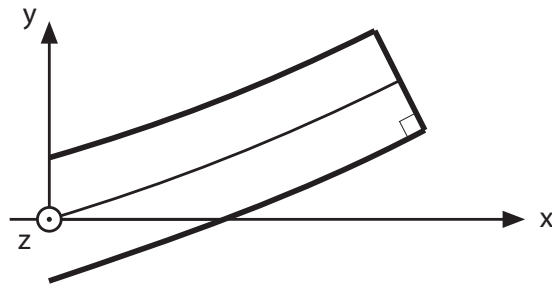


Figure 1.2. Cross section subjected to bending as utilized in Bernoulli-Euler Beam Theory [Andersen & Nielsen, 2008].

The general solution for the Bernoulli-Euler Beam Theory is Eq.(1.6).

$$\frac{d^4}{dx^4}u(x) = -\frac{q}{EI} \quad (1.6)$$

$u(x)$	Deflection [m]
q	Line load [N/m]

As seen in Eq.(1.6) shear stresses are not accounted for in Bernoulli-Euler Beam Theory. In order to account for the shear stresses, Timoshenko formulated the Timoshenko Beam Theory in 1921, [Andersen & Nielsen, 2008]. In order to account for this phenomenon, Timoshenko discarded the assumption from Bernoulli-Euler Beam Theory, which states that plane sections remain perpendicular to the neutral axis during bending, seen in Figure 1.3.

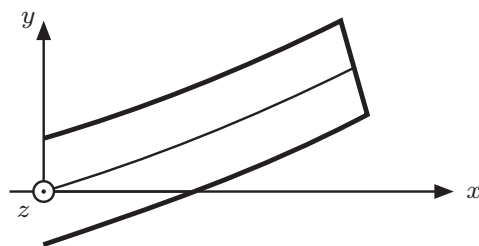


Figure 1.3. Cross section subjected to bending and shear which are the assumption for the Timoshenko Beam Theory [Andersen & Nielsen, 2008].

By adjusting the assumptions of the Bernoulli-Euler Beam Theory a term of shear stress is added to Eq.(1.6) as seen in Eq.(1.7).

$$\frac{d^4}{dx^4}u(x) = -\frac{q}{EI} + \frac{1}{GA} \frac{d^2 q}{dx^2} \quad (1.7)$$

G	Shear modulus [Pa]
-----	--------------------

However, as the actual cross section deforms as seen in Figure 1.4, both theories deviate from reality. As Figure 1.4 shows, the actual cross section deforms with a curve due to the shear stresses being largest at the neutral axis and decrease when approaching the edges of the cross section, [Andersen & Nielsen, 2008]. The shear stresses are neglected by Bernoulli-Euler Beam Theory and Timoshenko Beam Theory accounts for shear stresses from a plane effective cross sectional area. However, the deviation from reality decreases with the slenderness of the inspected column, as the shear stresses are increasingly smaller compared to the normal stresses.

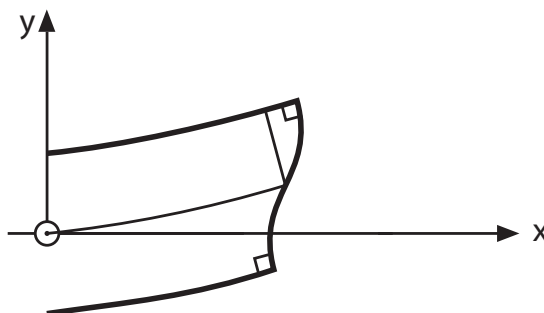


Figure 1.4. Actual deformation of a cross section subjected to bending [Andersen & Nielsen, 2008]

As this thesis focuses on general structural columns, which have high slenderness ratios, the Bernoulli Euler Beam Theory is assumed to be valid. In order to have a simple method to compare numerical results, the critical Euler load will be derived in the following section.

1.3 Derivation of the Critical Euler Load

A compression column, subjected to a constant normal force, N , with a constant stiffness, EI , is examined. A transient deformation, u_0 , is applied orthogonally to the normal force, causing a moment:

$$M = Nu_0 \quad (1.8)$$

If the column returns to its undeformed state, after the transient deformation is removed, the column is considered stable. If the normal force is increased to a point where the deformation becomes permanent, without buckling, the normal force applied is considered the critical Euler load, N_{cr} . If the load is increased further, the column will buckle, and global instability occurs, [Bonnerup et al., 2009].

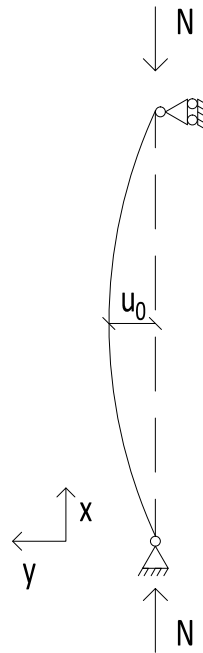


Figure 1.5. Simple supported column.

As the critical load is the point of interest, N_{cr} is derived for a simple supported column, seen in Figure 1.5. Through this assumption the bending moment can be expressed as the Bernoulli-Euler assumption, seen in Eq.(1.9).

$$M = -EI \frac{d^2y}{dx^2} \tag{1.9}$$

M	Bending moment [Nm]
E	Modulus of elasticity [Pa]
I	Moment of inertia [m ⁴]
$\frac{d^2y}{dx^2}$	Curvature [m]

A continuum is considered to obtain equilibrium and is illustrated in Figure 1.6.

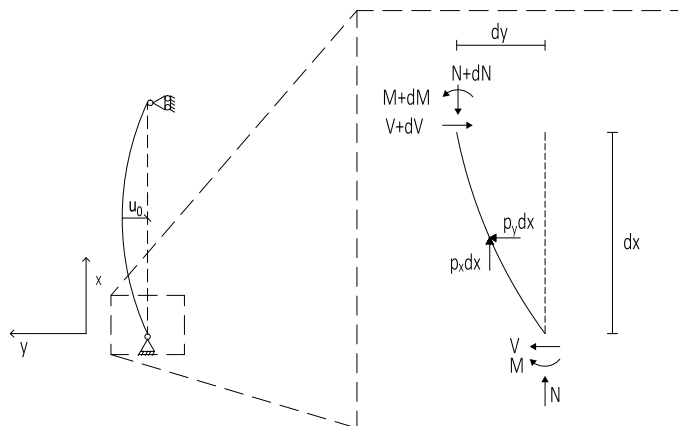


Figure 1.6. Increment of a column. [Bonnerup et al., 2009]

Equilibrium conditions are established as seen in Eq.(1.10) to (1.12).

$$N + p_x dx - (N + dN) = 0 \quad (1.10)$$

$$V + p_y dx - (V + dV) = 0 \quad (1.11)$$

$$M + dM - Vdx + Ndx + Ndy - M + p_x dx \left(\frac{1}{2}dy\right) - p_y dx \left(\frac{1}{2}dx\right) = 0 \quad (1.12)$$

The high order terms will be neglected and the terms are simplified.

$$\frac{dN}{dx} = p_x \quad (1.13)$$

$$\frac{dV}{dx} = p_y \quad (1.14)$$

$$\frac{dM}{dx} - V + N \frac{dy}{dx} = 0 \quad (1.15)$$

In order to obtain the differential equation for the column Eq.(1.9) and Eq.(1.14) are inserted into Eq.(1.15) and differentiated according to x. This will lead to the following equation.

$$\frac{d^2}{dx^2} \left(EI \frac{d^2y}{dx^2} \right) + \frac{d}{dx} \left(N \frac{dy}{dx} \right) = p_y \quad (1.16)$$

Assuming the stiffness, EI , and the normal force, N , does not change along the column, the transverse load, p_y is set equal to zero in the case of a uni-axial compressed column. From these assumptions the following differential equation is derived.

$$\frac{d^4y}{dx^4} + \frac{N}{EI} \frac{dy^2}{dx^2} = 0 \quad (1.17)$$

The boundary conditions for a simple supported column is given in the table below.

$$\begin{array}{l|l} y = 0 & x = 0 \wedge x = l \\ \frac{d^2y}{dx^2} = 0 & x = 0 \wedge x = l \end{array}$$

Based on these boundary conditions Eq.(1.17) is solved and the normal force is isolated. The critical Euler load is obtained.

$$N_{cr} = \frac{\pi^2 EI}{L_s^2} \quad (1.18)$$

$$\begin{array}{l|l} N_{cr} & \text{Critical Euler load [N]} \\ L_s & \text{Effective column length [m]} \end{array}$$

Eq.(1.18) calculates the critical load for the simplest form of global instability, which is Euler-buckling *i.e.* the first failure mode of the element.

In the before mentioned case, it is assumed that Hooke's Law is valid, *i.e.* Modulus of elasticity is constant, and thereby proportionality between stress and strain. This assumption is considered

valid for slender columns where the stresses are smaller than the proportionality limit. However, for short columns where the normal stress are larger than the proportionality limit, Modulus of elasticity will decrease as the stresses increase. As a consequence, when the effective length of the column approaches zero, the critical Euler load converges towards infinity.

As the critical Euler load is an idealized case and overestimates the load capacity, DS/EN 1993 demands that the stress-strain curve of the column, residual stresses and imperfections are considered as well.

1.4 Thesis Statement

As mentioned in the historical review, a number of different methods to account for imperfections in columns have been presented through the last couple of hundred years. This thesis seeks to compare the method of the current DS/EN standard to numerical models and experimental data found in literature. As indicated in the historical review, the perfect column does not correspond to reality, in which imperfections are impossible to prevent. In order to account for this, the DS/EN standard introduces an imperfection factor, α , which covers a variety of imperfections and load scenarios. Furthermore the DS/EN standard ensures sufficient safety of the structures by introducing the partial safety factor, γ_{M1} . As the partial safety factor in the DS/EN standard is defined identically for different load scenarios, this thesis seeks to calibrate a specific partial coefficient for simple supported steel columns subjected to weak axial bending caused by uni-axial compression and initial bow imperfections.

As the DS/EN standard covers a variety of different load scenarios related to columns, this thesis refrain from local instability and lateral torsional buckling. This thesis will thereby mainly focus on global buckling instability about the weak axis, caused by imperfections.

This leads to the following problems for investigation:

- How sensitive is the load capacity to varying imperfections and how does it provoke global buckling instability?
- How does the current methods of calculation in DS/EN correspond to experimental work and numerical models?
- How sensitive are the reliability index to varying stochastic variables?
- Is an optimization of the current partial safety factor in DS/EN for uni-axial compressed columns possible?

Part I

Buckling and Imperfection Study

2 Reference Geometry and material properties

The experimental data used for comparison in this thesis, is based on experiments conducted on simple supported IPE160 profiles in [Sfintesco, 1970]. Through this chapter, the reference geometry along with results obtained through the experiments will be presented.

2.1 Reference Geometry

The dimensions of the cross section for IPE160 profiles, are shown in Figure 2.1.

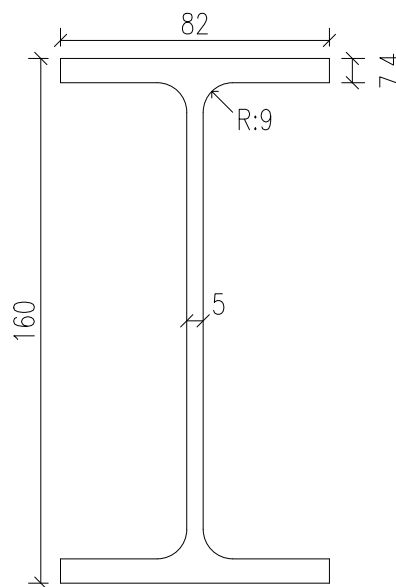


Figure 2.1. Nominal geometry of IPE160 profile.

A presentation of the geometrical and material properties can be seen in Table 2.1.

2.2 Reference material properties

In [Sfintesco, 1970], compression tests of three different steel column lengths of 12, 15 and 20 times the radius of gyration, i_y , of an IPE160 profile, corresponding to 0.8 m, 1.0 m and 1.3 m, are conducted in order to determine the modulus of elasticity and the yield strength of the material. The length of the test subjects are chosen in order to ensure material yielding and prevent global buckling.

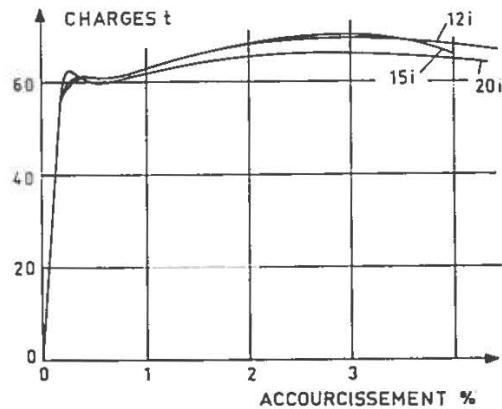


Figure 2.2. Performance curve for steel. [Sfintesco, 1970]

Figure 2.2 shows the deformation as a function of the load displayed in tons. As seen, the strength peaks at about 60 tons, corresponding to a yield stress about 300 MPa, which will be used as the ultimate yield stress through this part.

It is seen that the three test subjects follow the same elastic curve, which translate to a modulus of elasticity of 180 GPa. However, due to the poor quality of the figure, it is expected to have a considerable margin of error. A modulus of elasticity of 210 GPa will therefore be used, as [Jensen & Mohr, 2009] prescribes.

The geometry and material properties, used through the this part, are listed in Table 2.1.

Profile height, h	160	[mm]
Profile width, b	82	[mm]
Web thickness, d	5	[mm]
Flange thickness, t	7.4	[mm]
Cross sectional area, A	$2.01 \cdot 10^3$	[mm ²]
Moment of inertia, weak axis, I_z	$0.683 \cdot 10^6$	[mm ⁴]
Plastic moment of resistance, W_{pl}	$123.8 \cdot 10^3$	[mm ³]
Modulus of elasticity, E	$2.1 \cdot 10^5$	[MPa]
Ultimate yield stress, f_y	300	[MPa]
Poisson's ratio ν	0.3	[—]

Table 2.1. Material parameters and cross sectional dimensions [Jensen & Mohr, 2009].

2.3 Column Stability Experiments

A number of compression tests have been conducted as well. As opposed to the test subjects in the material tests, the following test subjects are sufficiently long to ensure global buckling. The test outcome can be seen in Table 2.2.

Number of tests	Slenderness ratio	Mean value	Standard deviation
	λ^* [–]	μ [kgf/mm ²]	σ [kgf/mm ²]
30	55	27.90	2.73
30	75	23.15	2.43
31	95	18.70	1.46
30	105	15.27	1.23
22	130	11.35	1.00
17	160	7.44	0.56

Table 2.2. Critical buckling results, acquired through experimental tests, [Sfintesco, 1970]

As seen in Table 2.2, the strength is presented in the unit [kgf/mm²]. In order to comply with modern standards, the parameters are converted to [MPa] and relative slenderness ratio. Furthermore the length of each test subject is calculated from the slenderness provided, using Eq.(2.1) and (2.2). The converted values are presented in Table 2.3.

$$i = \sqrt{\frac{I}{A}} \quad (2.1)$$

$$l = \lambda^* i \quad (2.2)$$

i	Radius of gyration [m]
λ^*	Slenderness ratio [–]
l	Length [m]

Number of tests	Relative	Length	Mean value	Standard	Variance
	slenderness ratio			deviation	
	λ [–]	[m]	μ [MPa]	σ [MPa]	$v = \frac{\sigma}{\mu}$ [–]
30	0.630	1.01	274.0	26.84	0.098
30	0.859	1.38	227.3	23.86	0.105
31	1.09	1.75	183.6	14.34	0.078
30	1.12	1.94	150.0	12.08	0.081
22	1.49	2.40	111.5	9.82	0.088
17	1.83	2.95	73.1	5.50	0.075

Table 2.3. Critical buckling results, acquired through experimental tests, presented by modern standards.

3 Load Capacity by DS/EN 1993-1-1

Through this chapter, the design method for columns in the current [DS/EN-1993-1-1, 2007] standard is reviewed.

3.1 Imperfections

In [DS/EN-1993-1-1, 2007] imperfections in each column are accounted for by an elastic imperfection reduction factor, α , which includes geometrical-, material imperfections and model uncertainties. Values for α are based on test results from [Maquoi & Rondal, 1978].

Depending on the geometrical properties of the column, α varies, as shown in Table 3.1.

Buckling curve	Imperfection factor α [–]
a_0	0.13
a	0.21
b	0.34
c	0.49
d	0.79

Table 3.1. Imperfection factors for buckling curves. [DS/EN-1993-1-1, 2007]

Stated in [DS/EN-1993-1-1, 2007], rolled profiles, with a relative slenderness ratio less than 1.2 and weak-axial bending, are considered to be column case b , corresponding to a cross sectional class 2, which yields an imperfection factor of 0.34.

When α has been chosen the column reduction factor, χ , which accounts for the reduction of load capacity in imperfect columns, can be calculated by Eq.(3.1).

$$\chi = \frac{1}{\phi + \sqrt{\phi^2 - \lambda^2}} \quad (3.1)$$

$$\begin{array}{l|l} \phi & 0.5(1 + \alpha(\lambda - 0.2) + \lambda^2) [-] \\ \lambda & \text{Relative slenderness ratio} [-] \end{array}$$

The reduction factor, as a function of column slenderness and imperfection factors, is shown in Figure 3.1, $\alpha = 0$ represents an idealized case with centrally loaded perfect columns, *i.e.* Euler-columns.

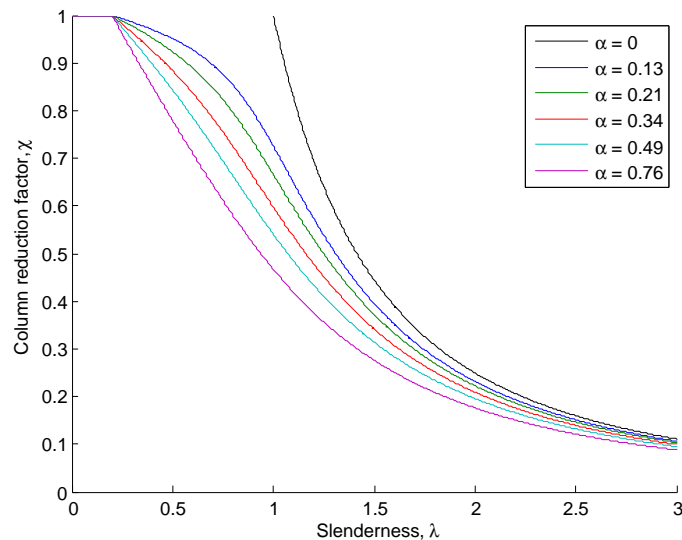


Figure 3.1. Imperfection factor

As the slenderness of a column increases, illustrated in Figure 3.1, the column reduction factor converges towards critical Euler-load, regardless of the imperfection factor.

3.2 Partial Safety Factor

[DS/EN-1990:2007, 2008] states two different methods of calculation for the design value of the load capacity. The Partial Safety Factor, $\gamma_{M,i}$ can be applied, either in the load capacity function, as seen in Eq. (3.2), or directly to the characteristic value, if the element is of a single material, shown in Eq. (3.3), which is suggested by 1993-1-1.

$$R_d = R \left\{ \eta_i \frac{X_{k,i}}{\gamma_{M,i}}; a_d \right\} \quad (3.2)$$

$$R_d = \frac{R_k}{\gamma_{M,i}} \quad (3.3)$$

R_d	Design resistance [Pa]
R_k	Characteristic resistance [Pa]
η_i	Conversion factor [—]
$X_{k,i}$	Characteristic value of the material [Pa]
$\gamma_{M,i}$	Partial safety factor [—]
a_d	Geometrical imperfection [m]

However, as statistical uncertainties are not introduced until Part II of this thesis, the partial safety factor will be left out through the load capacity calculations in Part I, in order to investigate the effects of imperfections.

3.3 Design Equations

In this section, the two design methods from the current [DS/EN-1993-1-1, 2007] will be reviewed. To determine the design equation for columns subjected to a normal force N_{Ed} and a bending

moment M_{Ed} Eq.(3.4) is derived from static equilibrium, [for Constructional Steelwork, 2006].

$$\frac{N_{Ed}}{N_{b,Rd}} + \frac{1}{1 - N_{Ed}/N_{cr}} \frac{N_{Ed}u_{0,d}}{M_{Rd}} + \frac{M_{Ed,II,max}^{II}}{M_{Rd}} \leq 1 \quad (3.4)$$

$M_{Ed,II,max}^{II}$	Design bending moment from the 2. order effect [Nm]
M_{Rd}	Design resistance [Nm]
u_0	Initial bow imperfection [m]

As it can prove problematic to determine the location of the maximum bending moment caused by the second order effect, $M_{Ed,II,max}^{II}$ is defined as seen in Eq.(3.5)

$$M_{Ed,II,max}^{II} = \frac{C_m M_{Ed,max}}{1 - N_{Ed}/N_{cr}} \quad (3.5)$$

C_m	Factor to account for 2. order bending moment effect [–]
$M_{Ed,max}$	1. order design bending moment [Nm]

Because the column can reach instability before yielding, M_{Rd} is replaced with $C M_{pl,Rd}$ where $M_{pl,Rd}$ is the fully plastic bending resistance and C account for axial force, slenderness of the profile and the distribution of the bending moment.

To determine the factor, C_m , [DS/EN-1993-1-1, 2007] states two different methods.

Method 1

Method 1 is derived on a theoretical basis and the different physical phenomenons are separated, which makes it easier to recognize the individual terms in the derivation. As Method 1 is a design method for general cases including limiting cases, this method must include more parameters to ensure a generalized formula. C_m is determined by Eq.(3.6).

$$C_{ii} = 1 + (w_i - 1) \left(2 - \frac{1.6}{w_i} C_{m,i}^2 (\lambda_{max} + \lambda_{max}^2) \right) \frac{N_{Ed}}{N_{pl,Rd}} \geq \frac{W_{el,j}}{W_{pl,i}} \quad (3.6)$$

λ_{max}	Highest relative slenderness [–]
w_i	The ratio between the plastic- W_{pl} and elastic modulus W_{el} [–]

Method 2

The concept of method 2 is to reduce the number of compact coefficients which makes it easier to apply to practical engineering. To derive C_m , numerical calculations are made, in order to recalculate the factor, so it fits buckling cases.

C_m is determined for weak axial bending by Eq.(3.7).

$$C_{mz} = 0.6 + 0.4\psi \geq 0.4 \quad (3.7)$$

ψ	The ratio between the two end moments [–]
--------	---

As method 1, according to [Bonnerup et al., 2009], overestimates the load bearing capacity of columns, and method 2 is preferred for practical engineering due to the simplicity of the expression, method 2 will be the preferred method through this thesis.

From these considerations, the global strength of columns is stated in [DS/EN-1993-1-1, 2007] as seen in Eq.(3.8) for weak-axial bending.

$$\frac{N_{Ed}}{\frac{\chi_z N_{Rk}}{\gamma_{M1}}} + k_{zz} \frac{M_{z,Ed}}{\frac{M_{z,Rk}}{\gamma_{M1}}} \leq 1 \quad (3.8)$$

N_{Ed}		Design normal force [N]
$M_{z,Ed}$		Design moment about weak axis [Nm]
χ_z		Column reduction factor [–]
k_{zz}		Interaction factor [–]

The interaction factor k_{zz} is determined, by Eq.(3.9).

$$k_{zz} = C_{mz}(1 + (2\lambda_z - 0.6)n_z) \leq C_{mz}(1 + 1.4n_z) \quad (3.9)$$

$$n_z = \frac{N_{Ed}}{\chi_z N_{pl,Rd}} \quad (3.10)$$

All analytical calculations from this point, will be based on Eq.(3.8).

4 Initial Finite Element Considerations

As this thesis is investigating the buckling point of a column subjected to uni-axial compression and bending moment, elements which can capture the physical behavior caused by both forces are preferable. Therefore, shell elements, a combination of membrane- and plate elements, which can capture both the deformation and the stresses in the element cross section, [Cook et al., 2002], are used through this thesis. The finite element analysis will be carried out in the commercial software Abaqus. In the Finite Element Analysis the geometry, presented in Section 2.1 is simplified, and will be carried out by a shell model with the cross section geometry shown in Figure 4.1.

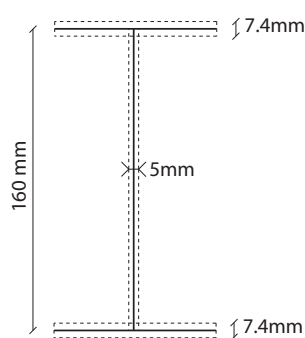


Figure 4.1. Shell geometry used in the Finite Element Model.

As seen in Figure 4.1, the shell model is slightly higher than the actual IPE160 profile, which causes a higher moment of inertia about the strong axis. However, as the column will be subjected to weak-axial bending, the effects from this deviation is assumed to be negligible, as

4.1 Shell analysis

Through this chapter different analysis types for numerical analysis in [DS/EN-1993-1-6, 2012] will be introduced. Though [?] covers shell constructions *e.g.* silos and other thin walled structures, the methods can be applied to shell elements used to model regular columns, as described in [DS/EN-1993-1-1, 2007] as well. The analyses which will be reviewed in this chapter concerns:

- Linear Elastic Analysis (LA)
- Linear Elastic Bifurcation Analysis (LBA)
- Materially Nonlinear Analysis (MNA)
- Geometrically Nonlinear Analysis (GNA)
- Geometrically and Materially Nonlinear Analysis (GMNA)
- Geometrically Nonlinear Analysis with Imperfections included (GNIA)
- Geometrically and Materially Nonlinear Analysis with Imperfections included (GMNIA)

Linear Elastic Analysis - LA

The Linear Elastic Analysis is based on the assumption of perfect geometry, linear elastic material law and small deformation theory. In small strain theory the deformation of the profile is assumed

to be significantly smaller than the profile dimensions, *i.e.* the geometry and the material properties in the cross section is assumed to be unchanged by the deformation. Through LA both compatibility in the deformations and equilibrium conditions must be satisfied.

Linear Elastic Bifurcation Analysis - LBA

Based on the same assumptions as LA, the linear bifurcation eigenvalue of a thin-walled shell profile is evaluated through LBA. Through this analysis several eigenmodes are revealed and the lowest bending eigenmode about the weak axis of the profile is chosen as the critical buckling load.

Materially Nonlinear Analysis - MNA

Similar to LA, MNA is based on the assumption of small strain theory and perfect geometry with nonlinear elasto-plastic material law, which means the load capacity of the profile will be limited by the yield stress of the material.

Geometrically Nonlinear Analysis - GNA

The GNA is based on the shell bending theory applied to a perfect structure with linear elastic material law. However, as opposed to LA, large strain theory is applied, *i.e.* deformations in the cross section are assumed to be relatively large compared to the profile dimensions. Due to the slenderness of column profiles, it is assumed that this analysis will not limit the load capacity of the profile.

Geometrically and Materially Nonlinear Analysis - GMNA

The GMNA is a combination of GNA and MNA. In this analysis shell bending theory is applied to a perfect structure. Displacements are assumed defined by nonlinear large strain theory and nonlinear elasto-plastic material law is applied.

Geometrically Nonlinear and Imperfection Analysis - GNIA

GNIA is similar to GNA and applies the same assumptions. However, in GNIA the profile deviates from the perfect geometry and imperfections are included. These imperfections can include initial bow imperfections, eccentricity of the load, nonlinear boundary conditions or effects of residual stresses.

Geometrically and Materially Nonlinear and Imperfection Analysis - GMNIA

GMNIA is identical to the GMNA analysis with imperfections included.

Table 4.1 shows a summary of the different analyses.

	Shell theory	Material law	Shell geometry
LA	Linear bending and stretching	Linear	Perfect
LBA	Linear bending and stretching	Linear	Perfect
MNA	Linear	Non-linear	Perfect
GNA	Non-linear	Linear	Perfect
GMNA	Non-linear	Non-linear	Perfect
GNIA	Non-linear	Linear	Imperfect
GMNIA	Non-linear	Non-linear	Imperfect

Table 4.1. Types of shell analysis according to, [DS/EN-1993-1-6, 2012]

Performance curves

Shown in Figure 4.2 are the seven different analysis types with increasing complexity. The results are shown for a simple supported column of 2.95 m in order to ensure that buckling occur with the purpose of showing the load capacity with each of the analysis types. The GNIA and GMNIA are conducted with an initial bow imperfection of 12 mm.

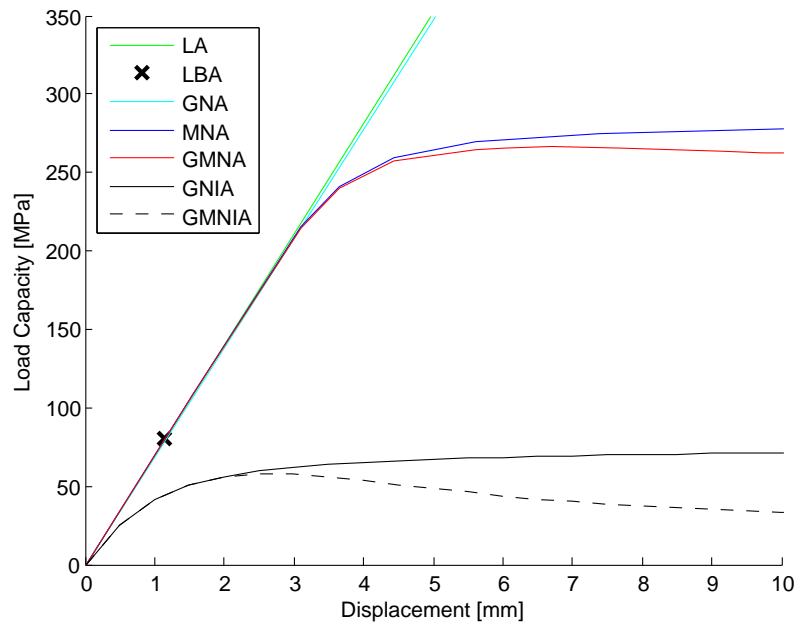


Figure 4.2. Performance curves from the varying analysis methods.

- The LA follows a strictly linear curve corresponding to the modulus of elasticity of the material.
- The bifurcation load found from the LBA is illustrated by the black cross.
- The MNA follows the LA in the elastic area and decreases in the modulus of elasticity as it approaches the ultimate yield stress.
- The GNA seems to be following the same linear curve, which can be explained due to the large strain theory the analysis follows. As the deformations in the cross section are much lower than the deformations in the axial direction of the column, the GNA will necessarily follow the LA very closely at small deformations.
- The GMNA follows both nonlinear geometry, *i.e.* large strain theory, and a nonlinear material law, which can be seen in the loss of load capacity when entering the plastic region.
- The GNIA and GMNIA analyses are visualized by the black solid and dashed lines respectively. It can be seen that, due to the imperfection, the load capacity for both the GNIA and GMNIA are significantly lower than what is the case of the same analyses without imperfections, GNA and GMNA.

Through this thesis, the GMNIA is the preferred shell analysis, while it, as opposed to the GNIA, allows material yielding, and will thereby give the most comparable results.

4.2 Numerical Solvers in Abaqus

Eigenvalue solver

When conducting a bifurcation analysis, in order to find the bending modes, the critical buckling loads are found from the nontrivial solution to the eigenvalue problem seen in Eq.(4.1)

$$\mathbf{K}^{M N} \bar{v}^M = 0 \quad (4.1)$$

$\mathbf{K}^{M N}$	Tangent stiffness matrix [N/m]
\bar{v}^M	Nontrivial displacement solutions [m]

Newton-Raphson Iteration Scheme

For a nonlinear analysis, two different cases exist, namely geometrical- and material nonlinearity. For both cases, the main problem is that the stiffness matrix does not remain constant, but changes with each load increment. When performing Finite Element Analyses a number of different iteration schemes may be used. In this section the Newton-Raphson iteration scheme will be reviewed, which uses iterations to obtain equilibrium between external and internal forces in the system. For the nonlinear equilibrium path, shown in Figure 4.3, the stiffness matrix is adjusted for each iteration step, in order to achieve equilibrium. The main concern with the Newton-Raphson iteration scheme, is that it has difficulties processing post-buckling behavior, where the slope of limit points are zero, illustrated in Figure 4.3.

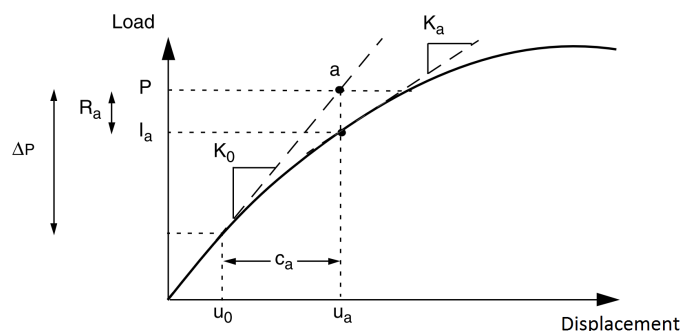


Figure 4.3. Principle sketch of the Newton-Raphson iteration scheme, [Corp., 1978].

However as the main focus of this project is initial buckling and as it is expected that columns will not obtain any additional post-buckling strength, a standard Newton-Raphson scheme will be used, through this project.

4.3 Boundary Conditions and loads

When considering one dimensional models, boundary conditions are fairly simple to design, as seen in Figure 4.4.



Figure 4.4. Simply Supported uni-axial compressed one dimensional column.

However, when considering models in three dimensions, the complexity of the models increase. As the Finite Element Model in this project involves shell analysis in three dimensions, the boundary conditions are described through this section.

In order to recreate a model as realistically as possible, a plate is attached to each end of the model. In reality, the plate will be bolted or welded to the column, as seen in Figure 4.5, the effects of these actions will, however, not be subject to analysis in this project.



Figure 4.5. Plate attached to the end of the column.[Constructalia, 2014]

In order to allow weak axial bending, the centerline of both column ends is fixed in the x- and y-direction, while it is allowed to move in the z-direction in one end of the column. The column is allowed to rotate freely, but due to the displacement fixities in both ends, the rotation stiffness of the column is relatively high and will therefore discourage torsional buckling, as seen Figure 4.6 and 4.7.

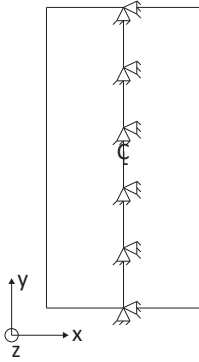


Figure 4.6. Boundary condition for the fixed end.

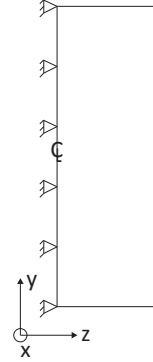


Figure 4.7. Boundary condition for the fixed end.

A forced displacement is applied in the centerline of one end of the column.

4.4 Shell Element Study

Two rectangular shell elements have been chosen for analysis in order to determine which element type suits the physical behavior of buckling best, namely the S4R and the S8R elements.

The S4R element, is a purely linear element with a node in each corner with three displacement- and three rotation degrees of freedom for each node. As the element is linear it has limitations regarding buckling, and more elements are needed in order to capture the bending shape of the profile, as seen in Figure 4.8.



Figure 4.8. Linear elements in bending.



Figure 4.9. Quad elements in bending.

The S8R element, has quadratic shape functions and can therefore capture bending shapes much more efficiently than the linear S4R elements, as seen in Figure 4.9. Furthermore the S8R element has four integration point whereas the S4R only has a single point. Therefore each S8R element is more time and resource consuming than each S4R element, however it is expected that the system will converge at fewer elements when using quadratic elements.

A convergence analysis for each element type will be conducted in order to determine which element is best suited for global instability studies. The analysis will be carried out for a 2.95 m, simple supported, IPE 160 profile with the same preferences as seen in Table 2.1 on page 14. Due to weak axial bending, the main influence of inaccuracies caused by element size is expected to be in the length direction of the column. As the LBA assumes small deformation theory, it is expected that the cross sectional mesh is of little importance. However, a convergence analysis in all directions will be conducted. In order to achieve a realistic result from the analysis and avoid an uneven distribution of integration points, it has been sought to maintain a length/width ratio of each shell element in the mesh between 0.2 and 5, therefore the initial convergence analysis will be conducted as shown in Table 4.2.

Element type	Flange	Web	Length
S4R	2	4	[32:256]
S4R	4	4	[64:256]
S4R	8	8	[64:512]
S8R	2	4	[32:256]
S8R	4	4	[64:256]

Table 4.2. Number of elements in the different profile directions. The two numbers in the length signifies the range of the convergence analysis.

The convergence will be presented by eigenvalue as a function of nodes, seen in Figure 4.10. Convergence is considered reached when the eigenvalue does not deviate more than 5 % when the number of elements is doubled.

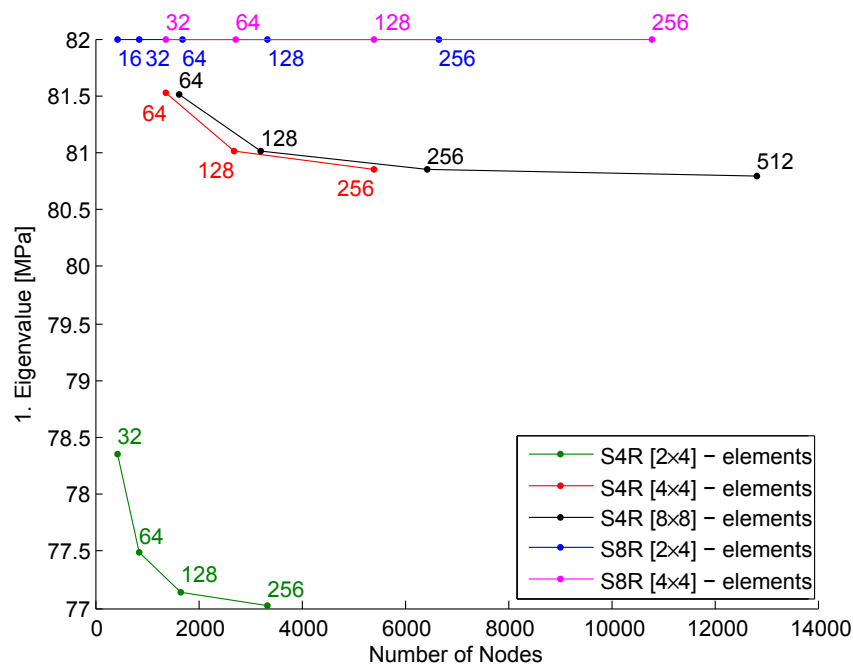


Figure 4.10. Convergence analysis for the first eigenmode.

As Figure 4.10 shows, the convergence analyses for the linear elements are less consistent than the convergence for the quadratic element. It is expected that the linear elements are not able to capture the cross sectional deformation, with a reasonable number of elements. As the S8R elements are visibly converged at a mesh with [2x4x32] elements, S8R elements are chosen for further analysis. The LBA assumes small strain theory, therefore a convergence analysis using GNA is required as well for the non-linear shell theories.

4.5 Verification of Mesh

Since GNA assumes large strain theory, a convergence analysis is necessary. As the GNA does not converge towards a specific stress point, as the LBA does, a different approach to convergence is considered. Three analyses will be conducted with varying number of elements in the length direction. The three different analyses will vary from two to eight elements in the flange as seen in Figure 4.11.

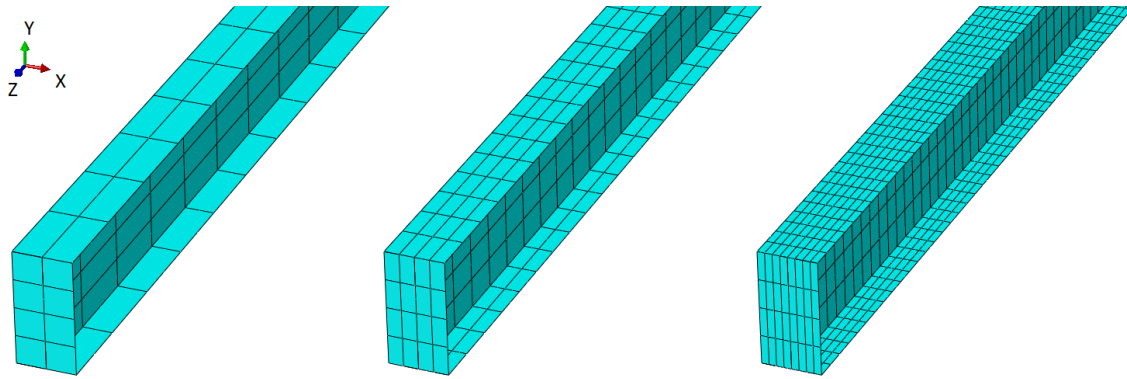


Figure 4.11. Shell model shown with varying mesh.

The number of elements in each direction is summarized in Table 4.3.

Flange	Web	Length
2	4	[32:256]
4	4	[64:256]
8	4	[128:256]

Table 4.3. Number of elements in the different profile directions. The two numbers in the length signifies the range of the convergence analysis.

The convergence analysis for the axial deformation at 235 MPa, as a function of the number of nodes, along with an analysis with the axial deformation as a function of the computational time, is seen in Figure 4.12 and 4.13.

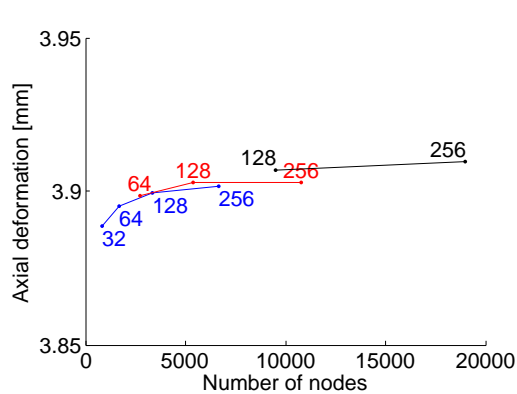


Figure 4.12. Convergence analysis for the axial deformation as a function of the number of nodes.

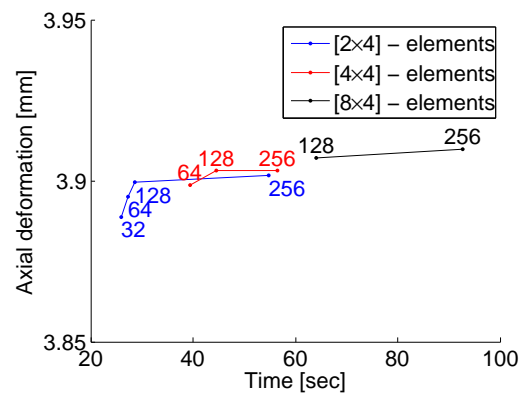


Figure 4.13. Convergence analysis for axial deformation as a function of computational time.

As seen, the axial deformation varies from approximately 3.89 mm to 3.91 mm. As the variation is no more than 0.5 % when the number of elements are doubled, the mesh is considered converged. As the computational time increases significantly, with the number of nodes in the model, the mesh is chosen as [2x4x32] S8R elements.

5 Imperfections in Finite Element

In structural columns, imperfections are not only seen as anomalies in the profile's geometry or material, but can also be introduced during installation [Schillinger et al., 1978]. Through this chapter, a study of different imperfections is performed in order to investigate the effect on the load capacity of the affected column.

This study will lead to a stochastic analysis in Part II of this thesis. The FERUM toolbox used in the stochastic analysis, requires a new Finite Element analysis, for each call to the limit state function. As this operation is ineffective, and not practically possible, an investigation of the influence of the different imperfections is conducted, in order to obtain a more effective solution. The imperfections chosen for this investigation in this thesis are:

- Initial bow imperfection
- Flange out-of-squareness imperfection
- High order eigenmode imperfection
- Yield stress imperfection
- Applied moment about one end
- Young's Modulus imperfection
- Combination
 - Bow- and out-of-squareness imperfection
 - Bow- and modulus of elasticity Imperfection
 - Bow- and yield stress imperfection

The imperfection analyses are conducted in Abaqus using GMNIA, and will be described in the following sections. The column geometry and material properties, are shown in Table 2.1 on page 14, applied to a 2.95 m simple supported column subjected to uni-axial compression.

5.1 Geometrical imperfections

During production, a variety of geometrical imperfections in a profile can occur. Through the manufacturing procedure, steel blocks are processed by rollers in order to obtain the desired geometry. After the initial rolling, the profile can be subject to a straightening process, in order to meet the required tolerances. However, as the perfect profile only exists in theory, imperfections will always be present. These imperfections can occur, *e.g.* when one or both rollers are out-of-line during rolling or by warping of the steel while cooling. Through the following sections, the three different geometrical imperfections, chosen for this thesis, will be studied.

5.1.1 Bow Imperfection

During the initial rolling of the profile, an initial bow imperfection is likely to be present, as seen in Figure 5.1. If the final straightening process is not done to perfection, this bow imperfection will remain and thereby cause a bending moment, as seen in Figure 5.2.

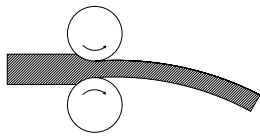


Figure 5.1. Principle sketch of the rolling process of steel profiles.

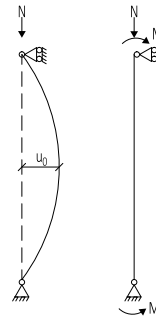


Figure 5.2. Bending moment caused by initial bow imperfection

In order to obtain the geometry desired for investigation of initial bow imperfections, an LBA is performed in Abaqus. Through this analysis, the first bending eigenmode, *i.e.* weak-axial bending, is acquired, and applied to the perfect geometry with a scaled amplitude, u_0 , seen in Figure 5.3

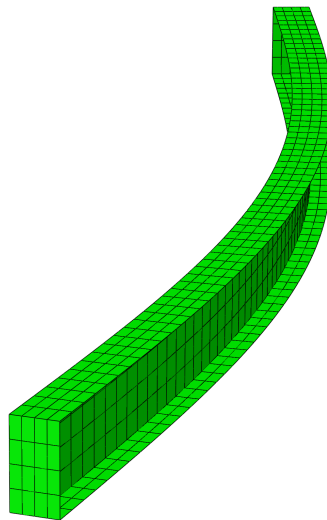


Figure 5.3. Scaled geometry of the profile subjected to initial bow imperfection, used in Abaqus.

A number of analyses are conducted in Abaqus, with increasing bow imperfection. From these analyses, the displacements in the load end of the column and reactions in the opposite, are extracted and performance curves, seen in Figure 5.4 are created.

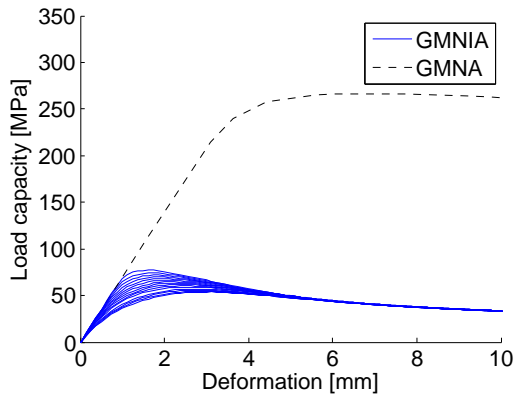


Figure 5.4. Stress-strain curve for a increasing bow imperfection.

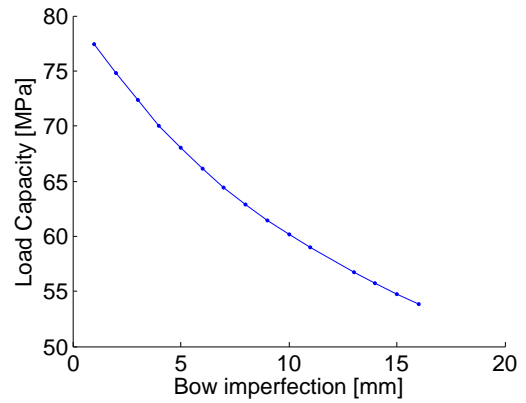


Figure 5.5. Load capacity shown as a function of initial bow imperfections.

Based on the performance curve, the load capacity at the buckling point of each bow imperfection amplitude is seen in Figure 5.5. It is seen that the load capacity drops significantly, when the bow imperfection is applied, due to the influence of the bending moment. This will cause the column to buckle about the weak axis, while the column without imperfection, will compress and cause local buckling, at a significantly higher load capacity, than what is the case when affected by global buckling.

The scaled deformed state of the profile can be seen in Figure 5.6, while the transparent mesh shows the initial geometry.

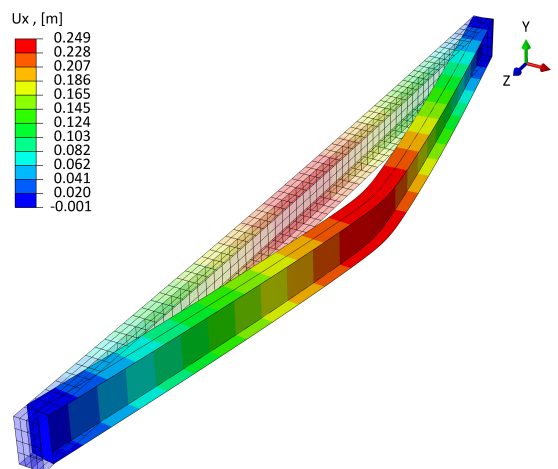


Figure 5.6. The deformed column with an initial bow imperfection.

5.1.2 Out-of-Squareness Imperfection

In order to review the effects from out-of-line rollers during the manufacturing process, an out-of-squareness imperfection is introduced in the cross section, as seen in Figure 5.7 and 5.8.

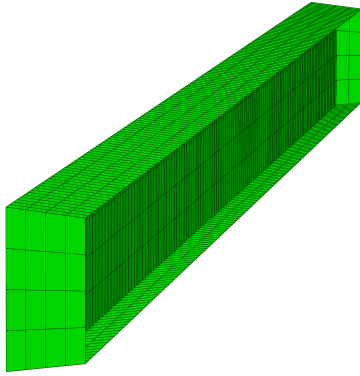


Figure 5.7. Out-of-squareness imperfection shown in the entire length of the profile.

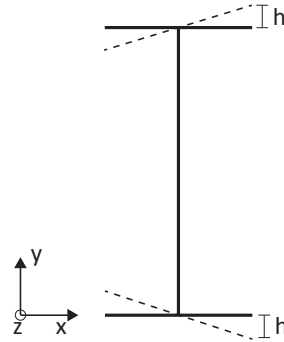


Figure 5.8. Principle sketch of the out-of-squareness imperfection applied to the cross section.

Shown in Figure 5.9 and 5.10, are the performance curve and load capacity as a function of the out-of-squareness imperfection.

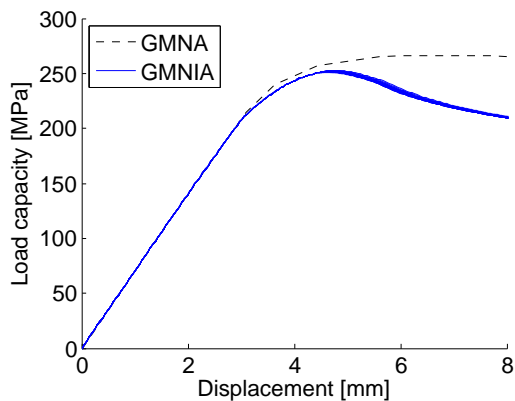


Figure 5.9. Performance curve for an increasing out-of-squareness imperfection.

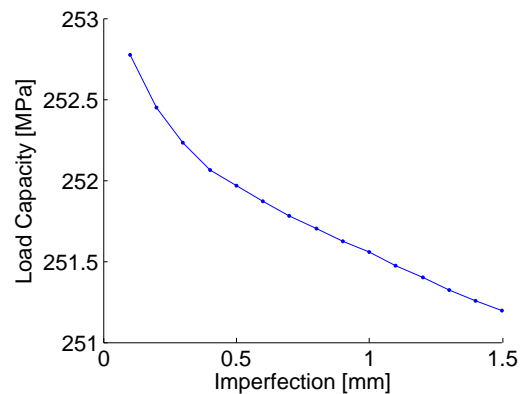


Figure 5.10. Load capacity shown as a function of out-of-squareness imperfection.

It is seen that no significant loss of load capacity can be observed when applying the out-of-squareness imperfection. As it is seen, the load capacity is not very sensitive to the out-of-squareness imperfection, which will therefore not be subject to any further individual investigations. The deformed state after failure of the profile subjected to an out-of-squareness imperfection can be seen in Figure 5.11. It is seen that no global buckling is present, however local buckling is seen in each end of the web.



Figure 5.11. The deformed column with an initial out-of-square imperfection.

5.1.3 High Order Eigenmode Imperfection

In order to investigate an imperfection, caused by rollers, which are not perfectly circular and rotating about an uneven axis, a high order eigenmode imperfection is applied to the perfect geometry. The imperfection is simulated in Abaqus, similarly to the bow imperfection, where an eigenmode is extracted from LBA. In order to contain the imperfection to the flanges, the web is constrained for all deformations in the LBA, while the flanges are allowed to deform freely. The deformed state of the eigenmode number 40 is applied to the perfect geometry, and the web is allowed to deform again. The initial geometry of the profile with eigenmode 40 imperfection applied, is shown in Figure 5.12.

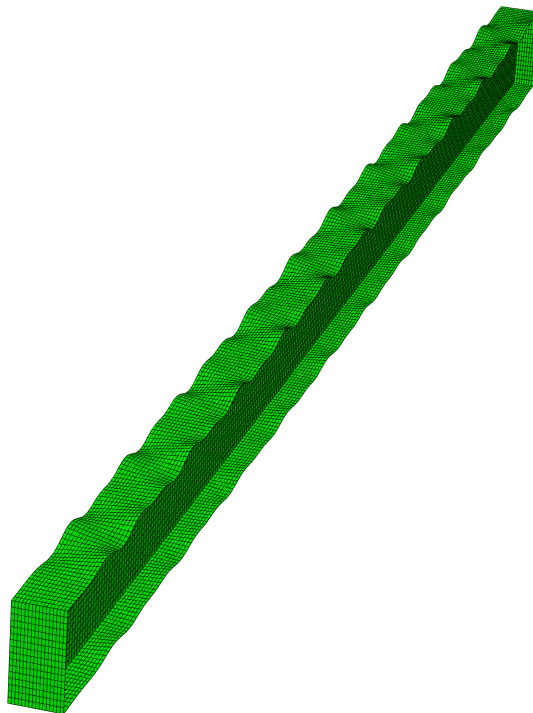


Figure 5.12. Initial geometry of eigenmode 40 imperfection applied to the profile.

The performance curves are shown in Figure 5.13, while the load capacity as a function of the imperfection amplitude is shown in Figure 5.14.

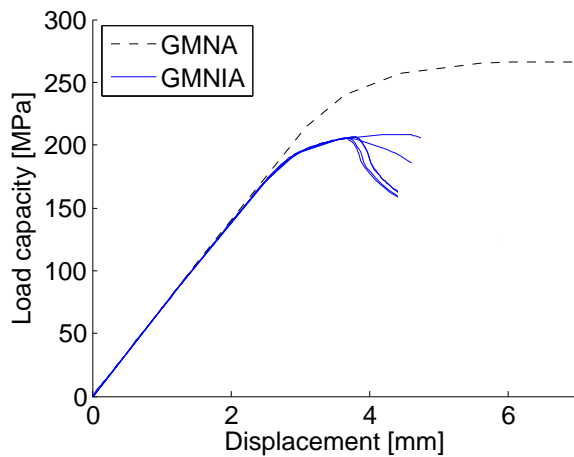


Figure 5.13. Stress-strain curve for eigenmode 40.

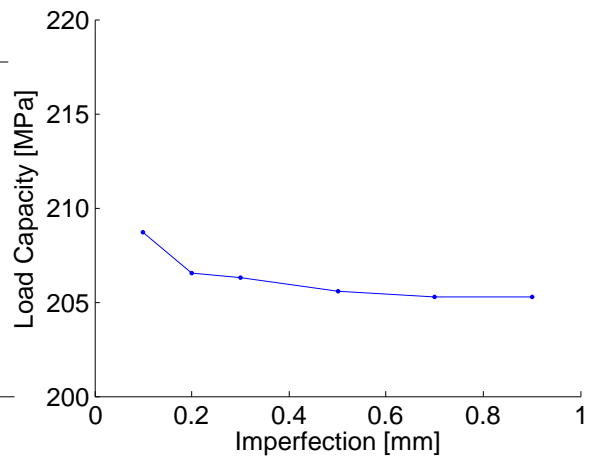


Figure 5.14. Load capacity for eigenmode 40.

Figure 5.14 shows, a significant drop in load capacity when the initial imperfection is applied. However, the amplitude of the imperfection is of little importance.

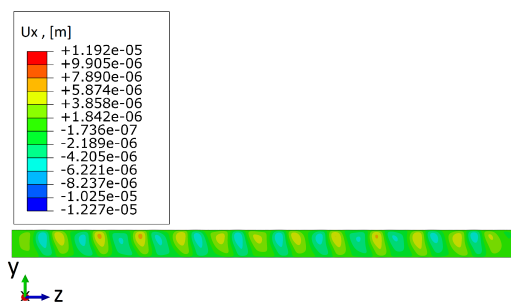


Figure 5.15. Deformations shown in the global x-direction in the web.

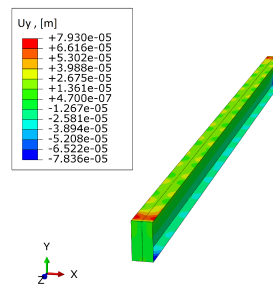


Figure 5.16. Deformations shown in the global y-direction in the flange.

Due to the imperfection being an out-of-squareness imperfection, it could be expected that the performance curve would be similar to the imperfection shown in the last section. However, while the imperfection in the last section is constant along the length of the profile, the imperfection varies significantly for the high order eigenmode imperfection. Due to this variation, the profile is susceptible to local buckling due to the moment introduced in local areas, which causes the initial drop in load capacity. The deformed state after failure can be seen in Figure 5.15 and 5.16 where, local buckling is seen in the web and flange respectively.

5.2 Material imperfections

Material properties can vary depending on supplier and quality. Through this section, the material properties are assumed homogenous for each profile, and will vary between each numerical simulation.

5.2.1 Modulus of elasticity Imperfection

To investigate the influence of a variation in the profile elasticity the same analysis as in the previous subsection is performed with a varying modulus of elasticity. The load capacity is shown in Figure 5.17.

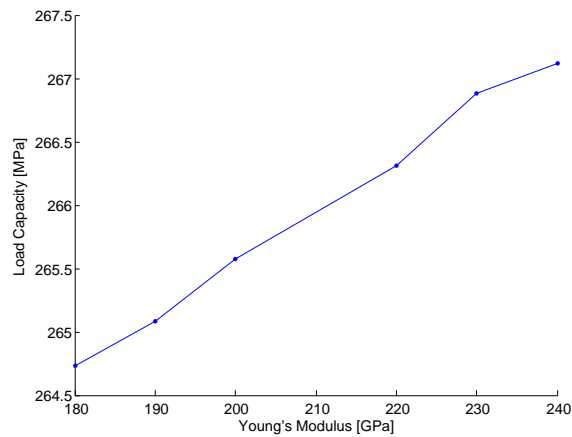


Figure 5.17. GMNA performed with a varying modulus of elasticity

From the variation of the load capacity as a function of the modulus of elasticity, shown in Figure 5.17, it is seen that the modulus of elasticity is of very little influence.

5.2.2 Yield Stress Imperfection

To investigate the influence of the yield stress a GMNA is performed with a varying yield stress. The load capacity is shown in Figure 5.18.

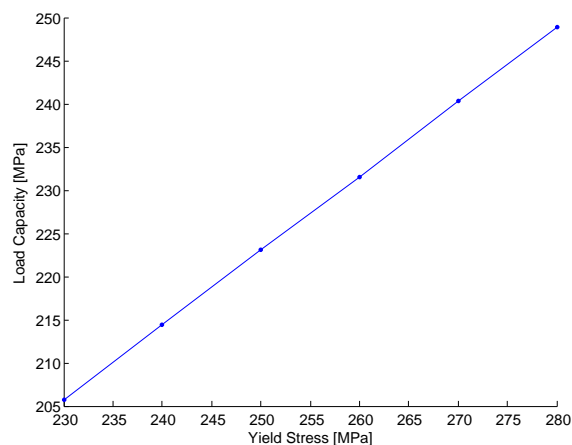


Figure 5.18. GMNA performed with a varying yield stress

Shown in Figure 5.18 it is seen that the load capacity as a function of varying yield stress, is increasing linearly, which indicates a proportionality between the yield stress and the load capacity.

5.3 Installation imperfections

Installation imperfections can lead to an extra bending moment, similarly to the bow imperfection, caused by load eccentricity, which will be the subject of investigation through this section.

5.3.1 Forced Rotation Imperfection

The load eccentricity will be simulated in Abaqus by applying a forced rotation about the weak axis in one end of the column. The load capacity as a function of the forced rotation is shown in Figure 5.19.

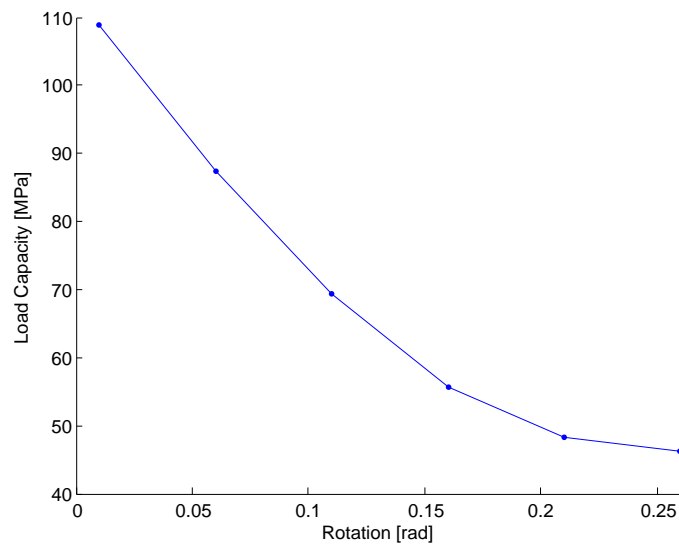


Figure 5.19. Load capacity shown as a function of increasing forced rotation.

The deformed state after failure is seen in Figure 5.20.

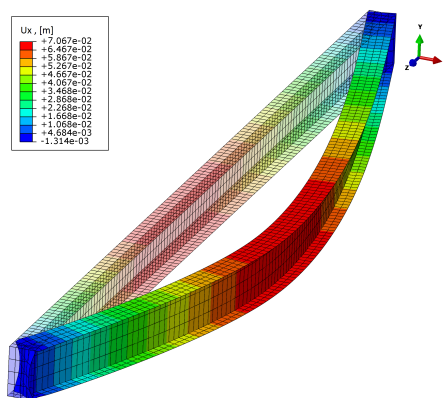


Figure 5.20. Deformed column subjected to a forced rotation about the weak axis in one end.

It is seen that the deformed state is not identical to the deformed state for the initial bow imperfection, which is caused by the eccentricity of the load, applied as a moment about just one end of the column. As a consequence, the largest deformation is displaced slightly from the middle of the column.

5.4 Combinations

Through this section, three combinations of two different imperfections, applied to a column simultaneously, is investigated. This investigation is conducted in order to see if any amplification of the imperfections occur compared to the imperfections applied individually. In order to study the influence of the combined imperfections, two separate studies of each combination will be presented. In each study, the initial bow imperfection will be fixed, according to the accepted tolerance, *i.e.* $0.03\% \cdot l \rightarrow 8.8 \text{ mm}$, [BS/EN-10034-1993, 1993].

5.4.1 Bow- and Out-of-Squareness Imperfection

Through this section the effects of combined bow- and out-of-squareness imperfection will be studied. The load capacity as a function of the imperfections can be seen in Figure 5.21 and 5.22. The out-of-squareness imperfection deviates from perfect squareness to the accepted tolerance of 0.75 mm according to [BS/EN-10034-1993, 1993].

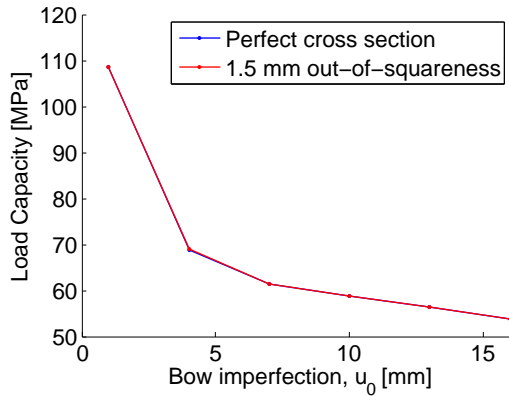


Figure 5.21. Performance curve of the load capacity as a function of the bow imperfection, shown for an out-of-squareness of 0 and 1.5 mm.

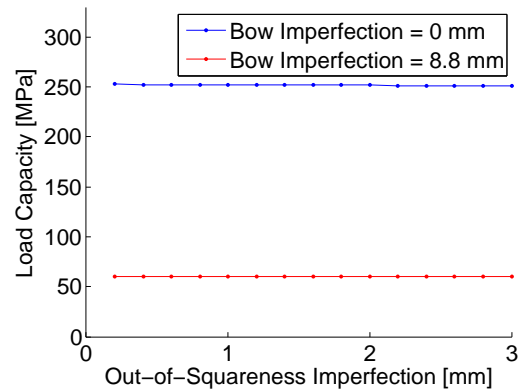


Figure 5.22. Performance curve of the load capacity as a function of the out-of-squareness, shown for a bow imperfection of 0 and 8.8 mm

As seen in the figures, the bow imperfection is highly dominant. From Figure 5.21 it is seen that the load capacity is unchanged when applying the tolerated deviation of out-of-squareness. In Figure 5.22 a large deviation from the perfect column to tolerated bow imperfection is obvious. From this study it is concluded that the bow imperfection is of far greater influence than the out-of-squareness imperfection and will therefore be subject to further study with a varying material parameter.

5.4.2 Bow- and Modulus of Elasticity Imperfection

In the following subsection the bow imperfection is combined with a varying modulus of elasticity. The two studies of the imperfection combination is seen in Figure 5.23 and 5.24. The modulus of elasticity deviates from the mean value 210 GPa, with the standard deviation, stated by [JCSS, 2002], seen in Table 7.2 on page 48.

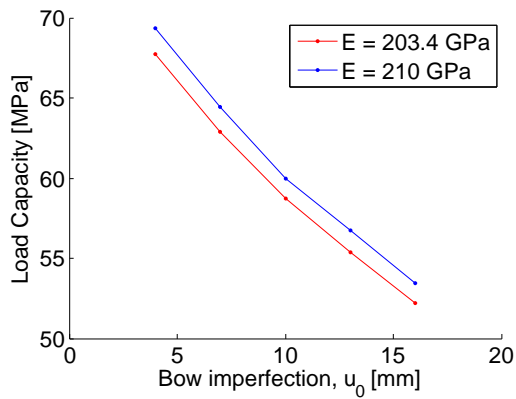


Figure 5.23. Performance curve of the load capacity as a function of the bow imperfection, shown for a modulus of elasticity of 203.4 and 210 GPa.

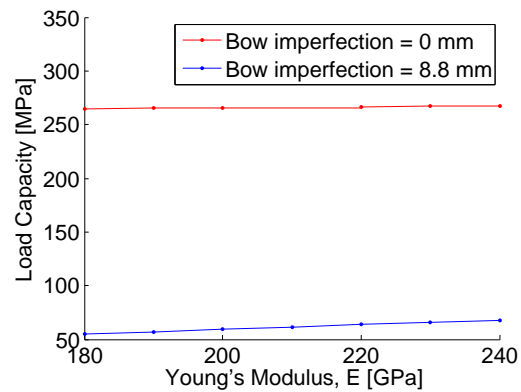


Figure 5.24. Performance curve of the load capacity as a function of the modulus of elasticity, shown for a bow imperfection of 0 and 8.8 mm.

It is seen that the modulus of elasticity is of little importance compared to the bow imperfection. The same study will be conducted for a combination of bow imperfection and yield stress in the following subsection.

5.4.3 Bow- and Yield Stress Imperfection

In the following subsection the bow imperfection is combined with a varying yield stress. The two studies of the imperfection combination is seen in Figure 5.25 and 5.26. The yield stress deviates from 300 MPa stated in Table 2.1 on page 14, with the standard deviation, according to [JCSS, 2002], stated in Table 7.2 on page 48.

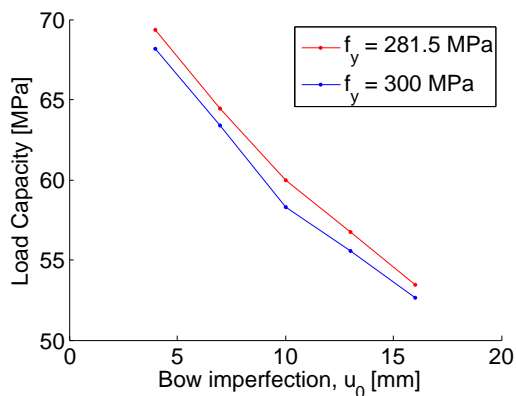


Figure 5.25. Performance curve of the load capacity as a function of the bow imperfection, shown for a yield stress of 300 and 281.5 MPa.

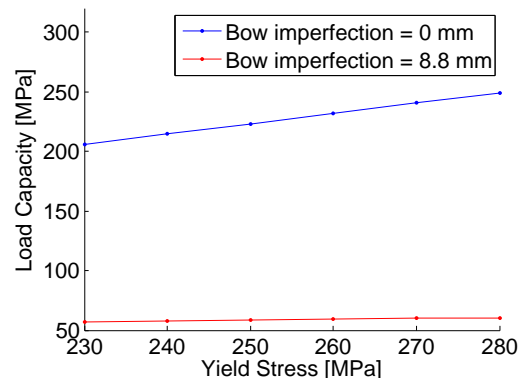


Figure 5.26. Performance curve of the load capacity as a function of the yield stress, shown for a bow imperfection of 0 and 8.8 mm.

Seen from the figures, the load capacity is not very sensitive to the variation of yield stress compared to the bow imperfection. However, as the reduction of the load capacity, seen in Figure 5.24 for the modulus of elasticity and 5.26 for yield stress, are larger for the varying yield stress in the interval of the standard deviation, this combination is chosen for further stochastic investigations in Part II of the thesis.

5.5 Data process for Stochastic chapter

In order to allow the use of two stochastic variables related to the profiles geometry and material, in the limit state function of the Finite Element Model, a surface plot of the load capacity as a function of the yield stress and bow imperfection will be obtained through this section. In order to assure that the interval is sufficiently large, the yield stress is chosen at an interval of 170-370 MPa, while the initial bow imperfection is chosen as 0-16 mm. From the analyses conducted in Abaqus, the following data shown in Figure 5.27 is obtained.

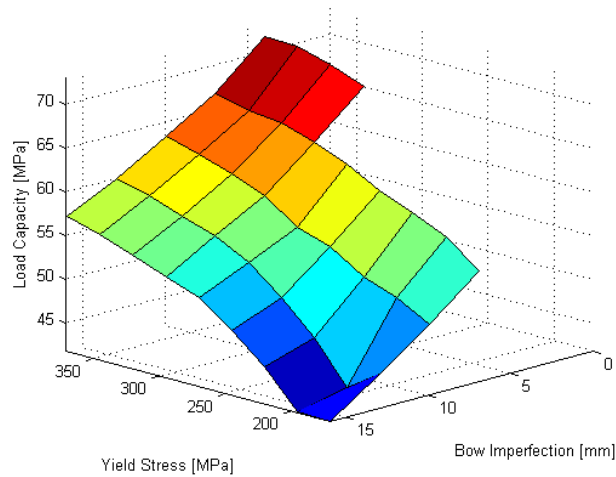


Figure 5.27. Load capacity of a 2.95 m column, subjected to a varying initial bow imperfection and yield stress.

In order to use for further stochastic analysis, an interpolation between the data points is required. Therefore a second order polynomial is fitted to the data points in each direction, and a surface is generated, seen in Figure 5.28.

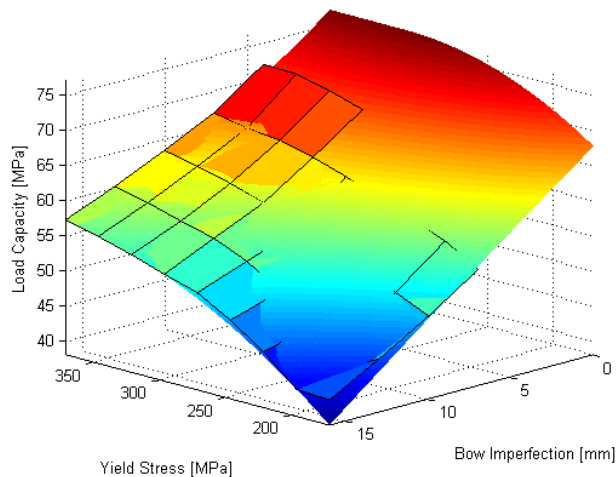


Figure 5.28. Simulated data, based on second order the polynomial, compared to the original data.

The comparison in Figure 5.28 verifies the validity of the second order polynomial. A comparison between the load capacity calculated by Finite Element Method, seen in Figure 5.27, and the load capacity calculated by the DS/EN method, seen in Eq.(3.8), can be seen in Figure 5.29.

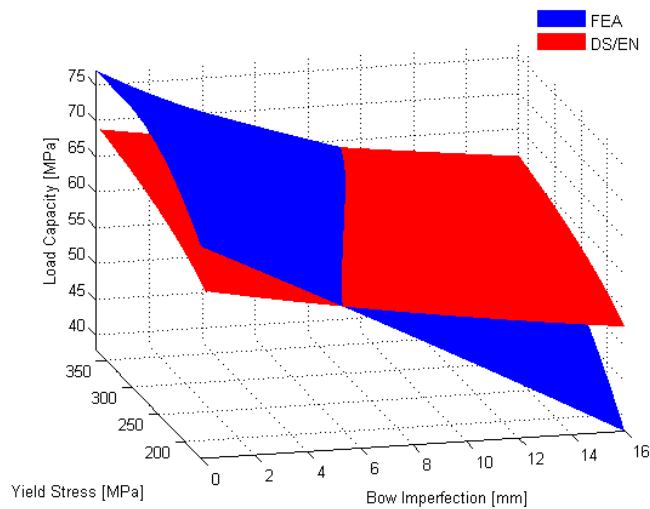


Figure 5.29. Load capacity for a column with varying yield stress, subjected to an increasing bow imperfection, based on FEA and DS/EN.

It is seen that the load capacity obtained through Finite Element Model is more susceptible to bow imperfections than the load capacity found through DS/EN calculations. As seen in Figure 5.29, the load capacity calculated by DS/EN is lower than the Finite Element Method, for imperfections below 6-10 mm, which corresponds well to the tolerance of $0.3\% \cdot l \rightarrow l/335$, according to [BS/EN-10034-1993, 1993], depending on the yield stress. This indicates that in order to obtain conservative results for the DS/EN method, the initial bow imperfection has to be in the interval below this tolerance level. However, according to [Bonnerup et al., 2009], DS/EN assumes an initial bow imperfection of $l/1000$ which is well under this tolerance level.

Part II

Stochastic Analysis

6 Model Uncertainty Estimation

The last part of the thesis treats imperfections as deterministic parameters, in order to investigate the influence each imperfection has on the load capacity. Based on these investigations it is recognized that bow imperfections are the most influential in relation to load capacity. Through this part, the bow imperfection, combined with the two stochastic material variables studied in Section 5.4, will be subject to stochastic analysis. In order to perform a stochastic analysis, a study of the uncertainties between the stochastic models and the experimental data is conducted. As the distribution of the acquired mean values and standard deviations, seen in Table 2.3 on page 15, is not stated, 160 column tests are simulated using a normal and lognormal distribution, in order to determine which distribution fits the experimental data best. With the simulated data, the bias is calculated as seen in the following section, based on the *Least Square Method* from [DS/EN-1990:2007, 2008], Annex D.8.

6.1 Calculation Method - DS/EN 1990, Annex D.8

Initially, the bias is calculated using, Eq.(6.1), which is used as the mean value for the model uncertainty in Chapter 7. The bias is an expression, quantifying the systematic error margin between the experimental- and theoretical data, seen in Figure 6.1.

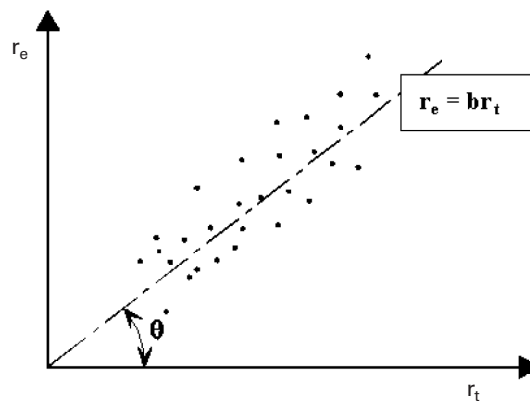


Figure 6.1. $r_e r_t$ diagram [DS/EN-1990:2007, 2008].

Each point in Figure 6.1, represents the relationship between an experimental data point, r_e , and theoretical data point, r_t . The line with angle, θ signifies the perfect fit, signifies the perfect fit between the theoretical and experimental data.

$$b = \frac{\sum r_e r_t}{\sum r_t^2} \tag{6.1}$$

b	Bias [—]
r_e	Experiments load capacity [Pa]
r_t	Theoretical load capacity [Pa]

Subsequently, a realization of the logarithmic model uncertainty of each simulated test point, Δ_i , is calculated, using Eq.(6.2).

$$\Delta_i = \ln \left(\frac{r_e}{b r_t} \right) \quad (6.2)$$

The standard deviation of the model uncertainty is estimated by Eq.(6.3).

$$s_{\Delta} = \sqrt{\frac{1}{N-1} \sum_{i=1}^N (\Delta_i - \bar{\Delta})^2} \quad (6.3)$$

s_{Δ}	Estimated standard deviation [Pa]
N	Number of tests
$\bar{\Delta}$	Mean value of the realization results [Pa]

The coefficient of variation of the model uncertainty, V_{Δ} , is calculated from Eq.(6.4).

$$V_{\Delta} = \sqrt{\exp(s_{\Delta}^2) - 1} \quad (6.4)$$

6.2 Model uncertainty for DS/EN

The load capacity, based on the DS/EN method and the experimental data generated from a normal- and a lognormal distribution, is compared in order to estimate the model uncertainty. The fitted data are shown in Figure 6.2 and 6.3 respectively. The theoretical load capacity is based on the same six column lengths, which were used in the experiments.

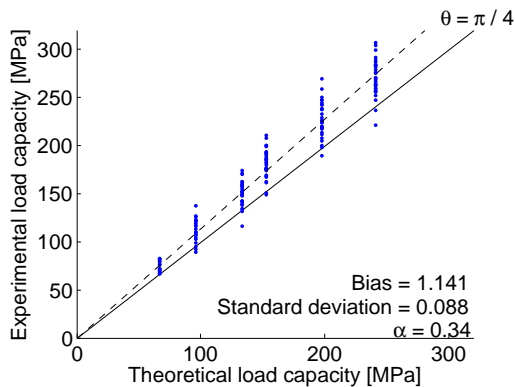


Figure 6.2. $r_e r_e$ diagram - Normal distribution.

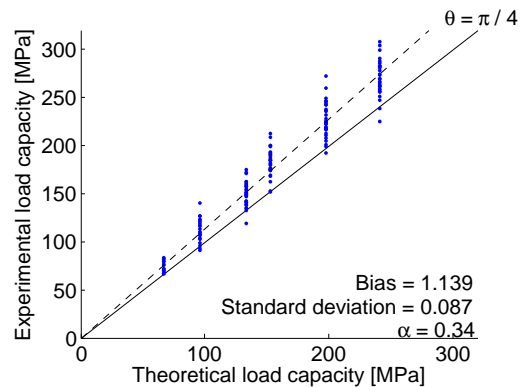


Figure 6.3. $r_e r_e$ diagram - Lognormal distribution.

As the two figures show, the model uncertainty based on the two distributions, are nearly identical. Therefore, a lognormal distribution is used, which is recommended by [DS/EN-1990:2007, 2008]. As expected the bias is above 1 which indicates that DS/EN method yields a conservative estimate of the load capacity, compared to the experimental data. The figures are shown for calculations for DS/EN without initial bow imperfection.

6.3 Model uncertainty for the Finite Element Model

In this section, the same experimental data, generated from a lognormal distribution, as was used in the previous section, is used to compare the Finite Element Model to the load capacity based

on the experiments. The numerical load capacity, is calculated using GMNIA, with an initial bow imperfection of $l/1000$, which is the considered initial bow imperfection according to [Bonnerup et al., 2009]. The relation between the numerical and experimental data is shown in Figure 6.4.

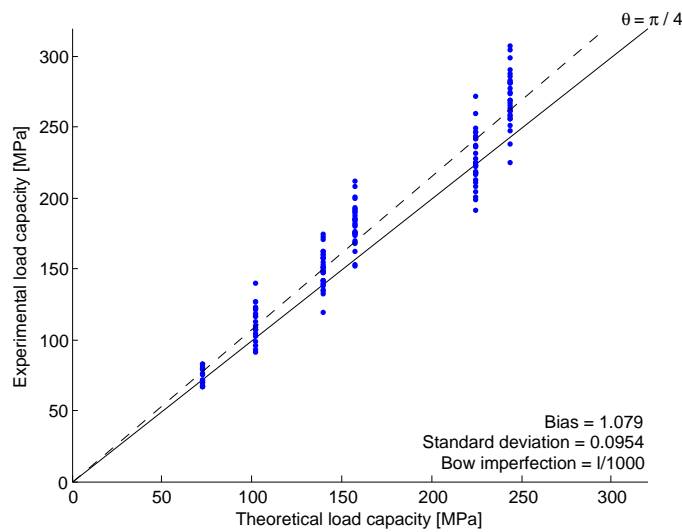


Figure 6.4. $r_e r_e$ diagram - Lognormal distribution.

The model uncertainty for the numerical model, shown in Figure 6.4, lies, as expected, between the DS/EN method and the experimental data. This leads to a hierarchic order of calculation methods as seen in Table 6.1.

Method of calculation	Resource consumption	Conservatism
DS/EN	Low	High
Numerical models	Moderate	Moderate
Experimental test	High	Low

Table 6.1. Hierarchic order of calculation methods

As standard based calculations are relatively resource efficient, it is often the method of choice for generalized cases in practical engineering. Therefore the calculations require a high level of reliability, *i.e.* conservative results, and thus yields the highest model uncertainty. For more complex problems, numerical models or experimental tests can be conducted, to ensure more realistic results. However, numerical or experimental models can be used for standard cases as well. As these more complex models are more resource demanding, a higher level of utilization of the load capacity, is desired in order to justify the use of the extra resources.

In the following chapter, the model uncertainty acquired for the DS/EN method and Finite Element Model will be used to calibrate the partial safety factor.

7 Stochastic Modeling

In this chapter, the stochastic variables, design equations and limit state functions are defined for both a uni-axial compressed column with and without an initial bow imperfection.

7.1 Stochastic Variables

In order to determine which parameters can be set as deterministic and which need to be stochastic, a sensitivity analysis of the model, with all parameters set at stochastic, should be performed. However, based on the studies of imperfections in Chapter 5, the stochastic and deterministic parameters are defined in the following subsections.

Geometrical

For the failure function defined by DS/EN the geometrical parameters, aside from the initial bow imperfection, are assumed to be deterministic.

Material distribution

Material parameters are usually considered either log- or normal distributed [Sørensen, 2004]. If the strength of a structure is defined with normal distributed variables the total strength will become normal distributed. This assumption is valid for ductile materials with small coefficients of variation. However, for a normal distribution with a high coefficient of variation the strength can become negative. To avoid this, a lognormal distribution can be considered, which is recommended by [DS/EN-1990:2007, 2008].

Load distribution

In this project, two loads are considered, dead- and snowload. These loads are chosen because they are considered to be the loads best suited to simulate column behavior by uni-axial compression. According to [DS/INF-172, 2009], the deadload is assumed to be normal distributed, while the snowload is assumed to be Gumbel distributed.

In this analysis, two different design load cases, based on (7.1) are considered, namely dominating deadload and domination snowload [DS/EN-1990:2007, 2008]. The partial safety factors of each load can be seen in Table 7.1.

	γ_{Dead}	γ_{Snow}
Dominating Deadload	1.5	0
Dominating Snowload	1	1.2

Table 7.1. Partial safety factors based on the dominating load.[NA:2013, 2013]

$$S = G_{dead}\gamma_{dead,i} + Q_{snow}\gamma_{snow,i} \quad (7.1)$$

G_{Dead}	Deadload [Pa]
Q_{Snow}	Snowload [Pa]
i	Dominating load case [–]
$\gamma_{Dead}, \gamma_{Snow}$	Partial safety factors [–]

Input parameters

In Table 7.2 the input parameter for the failure function defined by DS/EN shown.

		Distribution	Mean value	Standard deviation	Characteristic quantile	Reference
E	[GPa]	Lognormal	210	6.6	μ	[JCSS, 2002]
f_y	[MPa]	Lognormal	264	18.5	5 %	[JCSS, 2002]
G	[MPa]	Normal	1	0.1	50 %	[DS/INF-172, 2009]
Q	[MPa]	Gumbel	1	0.4	98 %	[DS/INF-172, 2009]
u_0	[m]	Normal	0	$l/1000$	50 %	[JCSS, 2002]
$x_{r,DS/EN}^{w/}$	[–]	Lognormal	1.14	0.087	-	[Figure 6.3]
$x_{r,DS/EN}^{w/o}$	[–]	Lognormal	1.16	0.087	-	[Figure 6.3]
$x_{r,FEA}$	[–]	Lognormal	1.08	0.095	-	[Figure 6.4]
I_z	[mm ⁴]	Deterministic	$0.683 \cdot 10^6$	-	-	[Jensen & Mohr, 2009]
W_{Pl}	[mm ³]	Deterministic	$123.8 \cdot 10^3$	-	-	[Jensen & Mohr, 2009]
A	[mm ²]	Deterministic	$2.01 \cdot 10^3$	-	-	[Jensen & Mohr, 2009]
l	[m]	Deterministic	2.95	-	-	[Sfintesco, 1970]
α	[–]	Deterministic	0.34	-	-	[DS/EN-1993-1-1, 2007]
c_{mz}	[–]	Deterministic	0.6	-	-	[DS/EN-1993-1-1, 2007]

Table 7.2. Stochastic variables, note that from this point forward, DS/EN is denoted w/ for calculations with initial bow imperfection and w/o without.

All parameters are assumed to be uncorrelated.

7.2 Design Equation

The design equation is the ratio between the resistance and the load, expressed by Eq.(7.2).

$$G = zR_d - S_d \quad (7.2)$$

R_d	Design resistance
S_d	Design load
z	Scale factor

In order to determine the design load, unit-loads are applied, while the load capacity of the column is scaled, using a scale-factor, z , until $G = 0$, and the design point is reached. The characteristic values and partial safety factors are used for Eq.(7.2) and when $G \leq 0$ failure will occur.

The design equation used is based on Eq.(7.3), from [DS/EN-1993-1-1, 2007].

$$\frac{N_{Ek}}{\frac{\chi f_{yk} A}{\gamma_{M1}}} + k_{zz} \frac{M_{Ek}}{\frac{W_{Pl} f_{yk}}{\gamma_{M1}}} = 1 \quad (7.3)$$

k_{zz}	Interaction factors [–]
W_{Pl}	The plastic moment of resistance [m ³]
f_{yk}	Characteristic yield stress [Pa]
γ_{M1}	Partial safety factor [–]
A	Cross sectional area [m ²]
χ	Column reduction factor [–]

However as the design equation is based on characteristic values, the equation can be significantly simplified. Seen in Table 7.2, the initial bow imperfection are normal distributed, has a mean value of zero, and the characteristic value is based on a 50 % quartile ,[Sørensen, 2004], *i.e.* the characteristic value is zero and the equation can be simplified to uni-axial compression, seen in Eq.(7.4).

$$\frac{N_{Ek}}{\frac{\chi f_{yk} A}{\gamma_{M1}}} = 1 \quad (7.4)$$

From Eq.(7.4), the design resistance is formulated for a column subjected to uni-axial compression, seen in Eq.(7.5).

$$R_d = \frac{\chi f_{yk} A}{\gamma_{M1}} = N_{Ed} \quad (7.5)$$

Seen in Eq.(7.5), the χ factor accounts for the imperfections in the otherwise perfect column.

The load term, S , is based on Eq.(7.1), with an added scale factor, η .

$$S = (1 - \eta)G_{dead}\gamma_{dead} + \eta Q_{snow}\gamma_{snow} \quad (7.6)$$

η	Scale factor between the dead- and snowload [–]
G_{Dead}	Deadload [Pa]
Q_{Snow}	Snowload [Pa]
$\gamma_{Dead}, \gamma_{Snow}$	Partial safety factors [–]

As the scale-factor, z , is used to scale the design resistance compared to the design load, η is introduced to scale the ratio between the dead- and snowload.

By inserting Eq.(7.5) and (7.6) into (7.2), the scale-factor, z , is obtained by setting $G = 0$.

$$G = z \left(\frac{\chi f_{yk} A}{\gamma_{M1}} \right) - ((1 - \eta)G_{dead}\gamma_{dead} + \eta Q_{snow}\gamma_{snow}) = 0 \quad (7.7)$$

In order to scale the loads in the design equation, a number of different η values, varying from zero to one is chosen. For each η value, a unique z value is calculated, and used to assign the dominating load in the limit state function, calculated in the following section. The design equation derived in this section, will be used for both the DS/EN and FEA limit state functions.

7.3 Limit State Function

The limit state function is used to determine the reliability index, β , of a model, compared to the design equation. The limit state function is defined by Eq.(7.8).

$$g = zRx_r - S \quad (7.8)$$

x_r | Model uncertainty - calculated in Chapter 6

For the limit state function the stochastic variables are used and no partial safety factors are applied. For the limit state function a failure surface is defined by $g(x) = 0$, seen in Figure 7.1. As seen in the figure, everything below the line, i.e. $g(x) > 0$ is considered safe, while $g(x) \leq 0$ is failure.

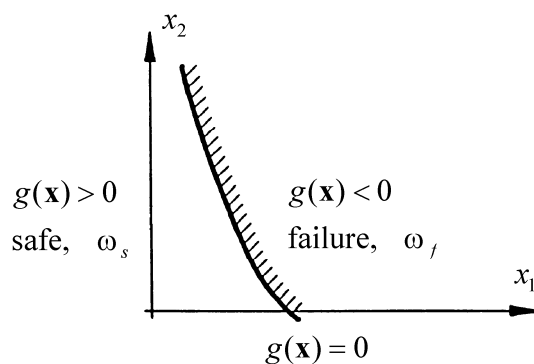


Figure 7.1. Limit state function [Sørensen, 2004].

DS/EN - Uni-axial compression

When dealing with a uni-axial compressed column the load capacity is found by Eq.(7.9).

$$R = \chi f_y A \quad (7.9)$$

The load, S , is defined by Eq.(7.10)

$$S = (1 - \eta)G_{dead} + \eta Q_{snow} \quad (7.10)$$

Thereby the limit state function for uni-axial compression is defined by Eq. (7.11).

$$g = z\chi f_y A x_r - ((1 - \eta)G_{dead} + \eta Q_{snow}) \quad (7.11)$$

DS/EN - Uni-axial compression with initial bow imperfection

When adding an initial bow imperfection to the limit state function an extra bending moment will occur. An extra moment term is therefore applied to Eq.(7.9), seen in Eq.(7.12).

$$\frac{N_E}{\chi A f_y} + k_{zz} \frac{M_E}{W_{Pl} f_y} = 1 \quad (7.12)$$

The bending moment is defined as the product of the normal force and the initial bow imperfection, expressed in Eq.(7.13).

$$M_E = N_E u_0 \quad (7.13)$$

When solving Eq.(7.12) two different solutions are obtained where one yields a negative load capacity, and is therefore discarded. The derivation of the limit state equation is found in Appendix A.

FEA - Uni-axial compression with initial bow imperfection

Through this analysis, the deterministic and stochastic parameters are chosen as seen in Table 7.2. However, as explained in Chapter 5, the only profile parameters considered stochastic, will be the initial bow imperfection and yield stress as these were the most influential parameters found in Section 5.4.

The limit state function, is based on Eq.(7.8), where the resistance, R , is expressed as a function of the initial bow imperfection and yield stress, seen in Figure 5.28 on page 39.

7.4 Reliability index

To estimate the reliability index of the limit state function, described in the previous section, different methods can be used. In this thesis, FORM (First Order Reliability Method) and MC (Crude Monte Carlo) method, will be used.

7.4.1 First Order Reliability Method

The concept of FORM is to linearize the failure surface of the limit state function, as seen in Figure 7.2 so a probability of failure can be estimated, [Sørensen, 2004].

In order to use FORM, the stochastic variables are transformed into the standard normally distributed variable \mathbf{U} with standard deviations of one and an expected value of zero. Thereby the probability of failure can be calculated with the standard normal distribution function, Φ , which is defined by Eq.(7.14).

$$P_f = \Phi(-\beta) \quad (7.14)$$

P_f	Probability of failure
Φ	Standard normal distribution function
β	Reliability index

The definition of the reliability index β is the shortest distance from origin to the failure surface $g(\mathbf{u}) = 0$ in the \mathbf{U} space, see Figure 7.2.

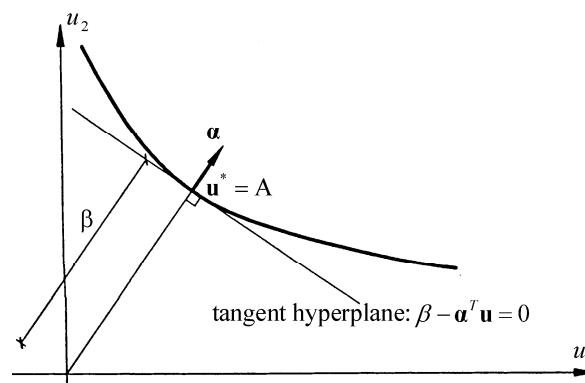


Figure 7.2. Reliability index[Sørensen, 2004].

7.4.2 Sensitivity Analysis

When the FORM analysis has estimated a probability of failure, a sensitivity analysis of each stochastic variable can be performed in order to give an estimation of how sensitive the reliability index is to any given stochastic variable.

In this thesis, the unit normal vector, α , to the failure surface at the design point, will be used to express the sensitivity. The α vector is expressed by Eq.(7.15).

$$\left. \frac{\partial \beta}{\partial u_i} \right|_{\mathbf{u}^*} = \alpha_i \quad (7.15)$$

α_i | Unit normal vector [–]

7.4.3 Crude Monte Carlo Simulation

The reliability index, calculated with FORM, is verified with the Crude Monte Carlo method. The Crude Monte Carlo, is a brute force method, which at a sufficient amount of simulations will converge towards a the correct reliability index, however it is very computationally heavy. The probability of failure is estimated by Eq.(7.16).

$$\hat{P}_f = \frac{1}{N} \sum_{j=1}^N I[g(\hat{\mathbf{u}}_j)] \quad (7.16)$$

\hat{P}_f	Probability of failure [–]
N	Number of simulations [–]
$I[g(\hat{\mathbf{u}}_j)]$	Indication function [–]
$g(\hat{\mathbf{u}}_j)$	Failure function [–]

The indication function is defined as:

$$I[g(\mathbf{u}_j)] = \begin{cases} 0 & \text{if } g(\mathbf{u}) > 0 \text{ Safe} \\ 1 & \text{if } g(\mathbf{u}) \leq 0 \text{ Failure} \end{cases} \quad (7.17)$$

The reliability index is calculated with the inverse standard normal distribution function Φ^{-1} and is defined with Eq.(7.18).

$$\beta = -\Phi^{-1}(P_f) \quad (7.18)$$

8 Stochastic results

In order to acquire the partial safety factors, the program FERUM is used to perform the stochastic analysis. The input parameters used in FERUM are described in Section 7.1. In the following section, calculations with the partial safety factor, according to the current Danish National Annex will be conducted through FORM and verified with Monte Carlo simulations. Subsequently a sensitivity analysis of the stochastic variables will be performed, in order to study the influence of the individual stochastic variable. Ultimately, the stochastic analyses, are used to calibrate the partial safety factor.

8.1 Reliability Analysis for the Current DS/EN Partial Safety Factor

Through this section, the reliability index, β , will be calculated for each of the three limit state functions. The reliability index for each limit state function will be calculated by FORM, and validated by Monte Carlo, shown in Figure 8.1

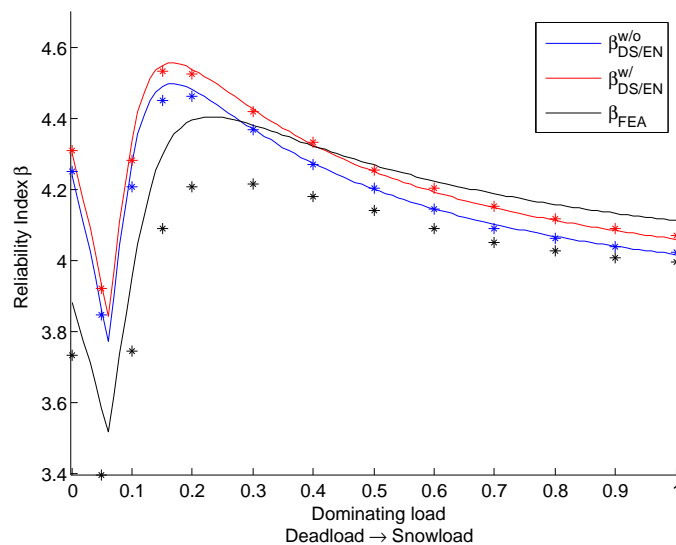


Figure 8.1. Reliability index shown for each of the three limit state functions, calculated by FORM and Monte Carlo, visualized by lines and asterisks respectively.

It is seen in Figure 8.1, the reliability method is stable, regardless if FORM or Monte Carlo is used. It is, however, seen that the reliability indices calculated by the FEA limit state function, deviates more than the DS/EN models. Nevertheless, as the tendency of the reliability indices are similar and deviates by no more than 0.2, the reliability is considered verified. The Monte Carlo method is confirmed by a convergence analysis of the probability of failure and the covariance of the probability of failure, seen in Figure 8.2 and 8.3.

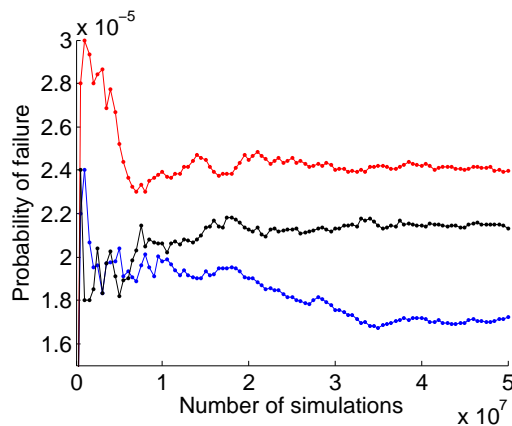


Figure 8.2. Probability of failure for the Monte Carlo method.

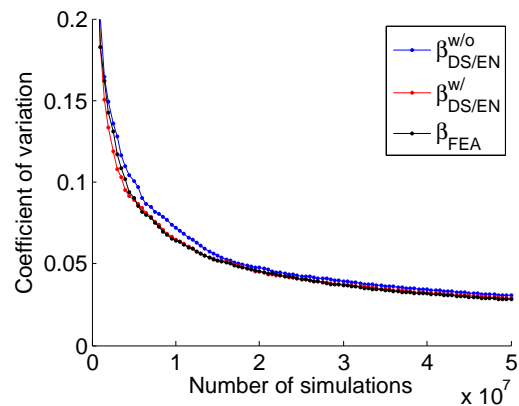


Figure 8.3. Covariance of the probability of failure of the Monte method.

As the reliability index has been verified, a sensitivity analysis is conducted and discussed in the following section

8.2 Sensitivity Analyses

Through this section, sensitivity analyses are conducted, in correspondence with Subsection 7.4.2. The analyses are conducted for the three limit state functions, in order to investigate the influence of each stochastic variable on the reliability indices. The analyses are presented for the limit state functions in Figure 8.4 for $DS/EN_{w/o}$, DS/EN_w and FEA respectively.

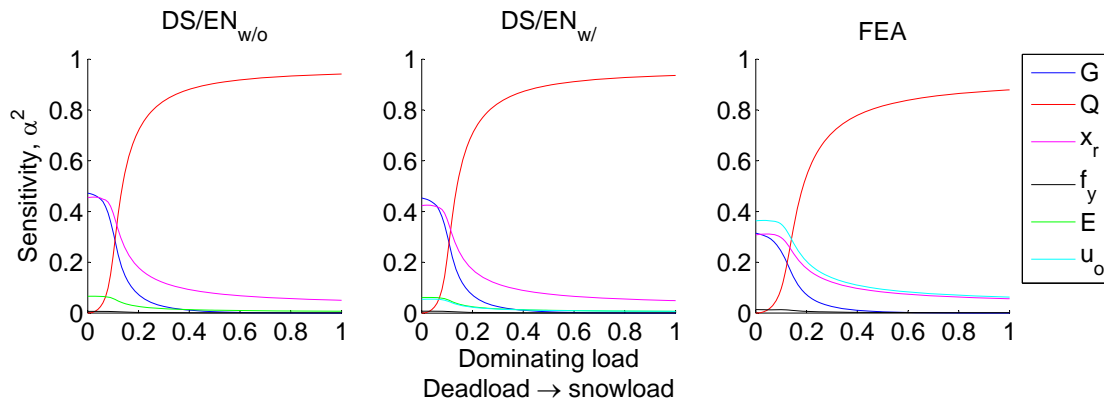


Figure 8.4. Sensitivity analysis for each of the three limit state functions.

The sensitivity analyses, shows that the reliability index becomes highly dependent on the snowload, for all limit state functions, while the yield stress is insignificant. Compared to the loads and the model uncertainty, it is seen that the initial bow imperfection is only of significance to the reliability in the FEA limit state function. However, as limit state functions contain a different number of stochastic variables, a definitive conclusion is difficult to reach. However, it is seen that the yield stress is generally insignificant. It is suspected that this is caused by the standard deviation of 18.5 MPa, which may be too low to cause any considerable impact on the reliability index, which is also indicated in Figure 5.29 on page 40.

8.3 Calibration of Partial Safety Factor

In order to calibrate the partial safety factor, γ_{M1} , the reliability indices are calculated with FORM for different γ_{M1} values for each weight factors. The target reliability index is chosen to 4.3, which according to the Danish National Annex is the one-year return period for consequence class 2.

To estimate the γ_{M1} corresponding the target reliability index, the partial safety factor, is calculated, based on the best fit in Eq.(8.1), [Hansen & Sørensen, 2002].

$$\gamma_{M1} \left(\min_M \right) = \sum (\beta_j(\gamma) - \beta_T)^2 \quad (8.1)$$

β_T | Target reliability index
 $\beta_{j,\eta}$ | The reliability index for each weight factor, η , at each iteration, j , of γ_{M1}

The plot of the margin of error, M as a function of γ_{M1} is seen in Figure 8.5 for each limit state function.

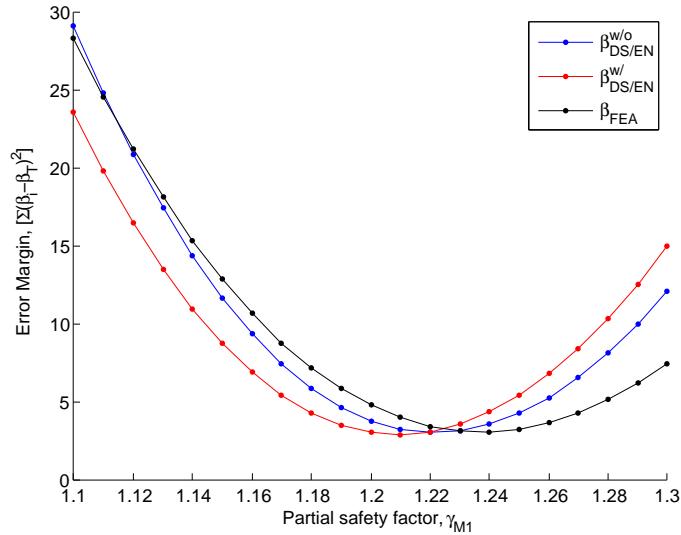


Figure 8.5. Margin of error for each iteration of the reliability index as a function of the partial safety factor.

The best fit between the reliability indices for each limit state function and target reliability index is seen to correspond to the Danish National Annex at about $\gamma_{M1} = 1.2$. The reliability indices as a function of the weight factor η , for the iterated γ_{M1} , are seen in Figure 8.6.

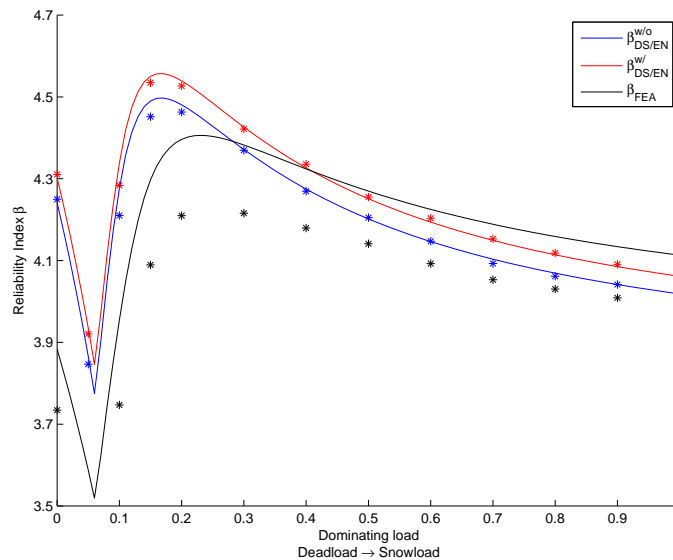


Figure 8.6. Reliability for each limit state function as a function of the weight factor.

The calibrated partial safety factor for each limit state function, in order to achieve the target reliability, is seen to be slightly higher than the National Annex suggests. This is suspected to be caused by a limited amount of uncertainties and stochastic variables. This will be subject to discussion in the following section.

8.4 Review of Results

The stochastic results obtained for the calibrated safety factor are seen in Table 8.1.

Design Eq. R = 65.1 MPa				
		DS/EN _{w/}	DS/EN _{w/o}	FEA
R	[MPa]	65.5	67.2	72.6
x_r	[-]	1.16	1.14	1.08
σ	[-]	0.087	0.087	0.095
$R \cdot x_r$	[MPa]	76.0	76.6	78.3
$\beta_m(\gamma_{M1} = 1.2)$	[-]	4.24	4.19	4.19
$\gamma_{M1}(\beta_T) = 4.3)$	[-]	1.20	1.22	1.24

Table 8.1. Summarization of results obtained through Chapter 8.

R	Load capacity
x_r	Model uncertainty
σ	Variation of the model uncertainty
$\beta_m(\gamma_{M1}=1.2)$	Reliability index
$\gamma_{M1}(\beta_T) = 4.3)$	Calibrated partial safety factor

The partial safety factor of the Finite Element method, is slightly higher than the safety factors obtained through DS/EN, as seen from Table 8.1. This is unexpected, as the load capacity found in the Finite Element Analyses in Part I, showed a higher load capacity which would be expected to cause lower partial safety factor. However, as the model uncertainty, accounts for the higher load

capacity, the deviation between the load capacities are evened out and the partial safety factors for each limit state function approaches the same value. In addition, the standard deviation of the model uncertainty is higher for the Finite Element Model, which reduces the reliability of the model, and thereby further increases the partial safety factor compared to the DS/EN models. In order to investigate this, the same stochastic analyses are conducted for unbiased models, which can be seen in Table 8.2.

Design Eq. R = 65.1 MPa				
		DS/EN _{w/}	DS/EN _{w/o}	FEA
R	[MPa]	65.5	67.2	72.6
x_r	[-]	1	1	1
σ	[-]	0.087	0.087	0.095
$R \cdot x_r$	[MPa]	65.5	67.2	72.6
$\beta_m (\gamma_{M1} = 1.2)$	[-]	3.51	3.54	3.84
$\gamma_{M1} (\beta_T = 4.3)$	[-]	1.44	1.41	1.35

Table 8.2. Unbiased results of the stochastic analyses.

The reliability index decreases which causes a higher required partial safety factor. However, the partial safety factor for the Finite Element Model is seen to be lower than the DS/EN models, which confirms the importance of the model uncertainty.

Furthermore, as the sensitivity analyses indicated, the snowload is highly dominant. An investigation is therefore conducted with the covariance of the snowload changed from 0.4 to 0.3. This should increase the reliability of the model and thereby decrease the required partial safety factor in order to obtain the target reliability. The results are shown in Figure 8.3. The models are again considered biased.

Design Eq. R = 65.1 MPa				
		DS/EN _{w/}	DS/EN _{w/o}	FEA
R	[MPa]	65.5	67.2	72.6
x_r	[-]	1.16	1.14	1.08
σ	[-]	0.087	0.087	0.095
$R \cdot x_r$	[MPa]	76.0	76.6	78.3
$\beta_m (\gamma_{M1} = 1.2)$	[-]	4.43	4.38	4.33
$\gamma_{M1} (\beta_T = 4.3)$	[-]	1.18	1.19	1.20

Table 8.3. Biased results obtained for a covariance of the snowload of 0.3.

As expected, the reliability index decreases, compared to the results shown in Table 8.1. Furthermore, when comparing the results for the model with a snowload with a covariance of 0.3 and the unbiased model with a covariance of 0.4, to the original results, it is seen that the partial safety factor deviates more for the unbiased model. This could indicate that the model uncertainty is of interest for further studies.

9 Conclusion

Through this thesis, global buckling of a uni-axially compressed simple supported column has been studied. The studies have been conducted through analytical and numerical analysis, which have been compared to experimental results. The analytical analysis is based on [DS/EN-1993-1-1, 2007], while the numerical models are conducted through the commercial software Abaqus. This has led to a study of a variety of imperfections in order to determine the influence on the critical buckling load of columns. Geometrical and installation imperfections are seen to be of greater influence to the load capacity than material variations. Especially bow imperfection and load eccentricity are seen to influence the critical buckling point as these provoke global instability, while the columns subjected to the other imperfections are more disposed to local instability. It is observed that the results of the DS/EN methods are conservative and can be increased by 5-10% compared to the numerical and experimental results. However, it is observed that the DS/EN model is less susceptible to bow imperfections, than the numerical model, as a consequence the load capacity at large bow imperfections is underestimated by the DS/EN method. However, according to [Bonnerup et al., 2009], the initial bow imperfection in structural columns, is considered to be significantly less than this tolerance level.

After the imperfection study, a comparison between the theoretical models and experimental data has been conducted in order to obtain the model uncertainty, for stochastic analysis. It is observed that the load capacity of the Finite Element Model, corresponds better to reality than the analytical models, which is reflected in a higher bias. However, the standard deviation of the model uncertainty is slightly higher.

Subsequently a FORM analysis is performed where the design equation is based on the [DS/EN-1993-1-1, 2007], in order to examine the reliability of the current standard. Three different limit state functions are defined based on [DS/EN-1993-1-1, 2007], with and without initial bow imperfection, and an imperfect numerical model using GMNIA. The stochastic analyses shows that the limit state functions are slightly unreliable, which is assumed to be a consequence of the relatively large standard deviation of the model uncertainty. As a result, a slight upward adjustment of the partial safety factor is suggested, based on the Danish National Annex. It is furthermore observed that the Finite Element Model yields a slightly higher partial safety factor than the analytical models, which is unexpected. Therefore an investigation of the model uncertainty is conducted. The same stochastic analyses are therefore performed with unbiased models, with the same standard deviation of the model uncertainty. As expected, it is seen that the Finite Element Model yields a lower partial safety factor.

As the partial safety factors are regarded as slightly high, the uncertainty of the distribution for the snowload is reviewed as well. As the snowload is seen to be highly dominant in the sensitivity analyses, the covariance is scaled down from 0.4 to 0.3, otherwise suggested by [JCSS, 2002]. As a results, the partial safety factor is reduced slightly, but is still within a very close range to the value suggested by the Danish National Annex. This suggests that a revision of the parameters used in the limit state functions could be subject to further analysis. However, based on the calculations conducted through this thesis, it is concluded that recommended values suggested by the Danish National Annex are accurately defined.

Bibliography

- L. Andersen & S. R. Nielsen (2008). *Elastic Beams in Three Dimensions*. Aalborg University.
- B. Bonnerup, et al. (2009). *Stålkonstruktioner efter DS/EN 1993*. Nyt Teknisk Forlag.
- BS/EN-10034-1993 (1993). *BS EN 10034-1993, Structural steel I and H sections, Tolerances on shape and dimensions*. Parker steel.
- Constructalia (2014). *Column end*. Constructalia.
- R. D. Cook, et al. (2002). *Concepts and applications of the Finite Element analysis*. Wiley & Sons. Inc.
- S. Corp. (1978). *Abaqus Analysis User's Guide*.
- DS/EN-1990:2007 (2008). 'Basis of Structural Design'.
- DS/EN-1993-1-1 (2007). 'Design of Steel Structures - General rules and rules for buildings'.
- DS/EN-1993-1-6 (2012). *Eurocode 3 : Stålkonstruktioner: Del 1-6 : skalkonstruktioners styrke og stabilitet*. DS/EN 1993-1-6+AC. Dansk Standard.
- DS/INF-172 (2009). 'Background investigations in relation to the drafting of National Annexes to EN 1990 and EN 1991 – Reliability verification formats, combination of actions, partial coefficients, fatigue, snowload, windload, etc.'.
- L. Euler & W. Oldfather (1933). *Leonh. Euler's Elastic Curves: (De Curvis Elasticis ; Additamentum I to His Methodus Inveniendi Lineas Curvas Maximi Minimive Proprietate Gaudentes, Lausanne and Geneva, 1744)*.
- E. C. for Constructional Steelwork (2006). *Rules for Member Stability in EN 1993-1-1: Background Documentation and Design Guidelines*. European Convention for Constructional Steelwork.
- P. F. Hansen & J. D. Sørensen (2002). 'Reliability-based code calibration of partial safety factors'. *JCSS*.
- T. Haukaas (2012). *Euler Bernoulli-Beams*. University of British Columbia.
- JCSS (2002). *Probabilistic Model Code*. Technical University of Denmark.
- B. Jensen & G. Mohr (2009). *Teknisk ståbi*. Nyt Teknisk Forlag.
- B. Johnston (1983). 'Column Buckling Theory: History Highlights'. *Journal of Structural Engineering*.
- R. Maquoi & J. Rondal (1978). 'Stahl: Eigenschaften, Verarbeitung und Anwendung von Stahl'. *Analytische Formulierung der neuen Europäischen Knickspannungskurven*.
- D.-. D. NA:2013 (2013). *Eurocode 0: Projekteringsgrundlag for bærende konstruktioner*. Dansk Standard.

- V. Papadopoulos, et al. (2012). 'Buckling analysis of I-section portal frames with stochastic imperfections'. *Engineering Structures* .
- D. Schillinger, et al. (1978). 'Buckling analysis of imperfect I-section beam-columns with stochastic shell finite elements'. *Computational Mechanics, Volume 46, Issue 3, pp 495-510* .
- P. D. Sfintesco (1970). 'Fondement Expérimental Des Courbes Européennes De Flambement'. *Construction métallique* .
- F. Shanley (1947). 'Inelastic Column Theory'. *Journal of Aeronautical Science, Vol. 14, No. 5* .
- J. D. Sørensen (2004). *Notes in Structural Reliability Theory And Risk Analysis*. Aalborg University.
- A. Stavrev, et al. (2013). 'Comparison of Eigenmode-Based and random field-based imperfection modeling for the stochastic buckling analysis of I-Section Beam-Columns'. *International Journal of Structural Stability and Dynamics* .
- T. Usami & Y. Itoh (1998). *Stability and Ductility of Steel Structures*. Elsevier Science.
- P. Van Musschenbroek (1729). *Physicae experimentales, et geometricae: de magnete, tuborum capillarum vitreorumque speculorum attractione, magnitudine terrae, cohaerentia corporum firmorum : dissertationes ut et ephemerides meteorologicae Ultrajectinae*. S. Luchtmans.
- R. Ziemian (2010). *Guide to Stability Design Criteria for Metal Structures*. John Wiley & Sons.

A Limit state function

In this appendix the limit state function and design equation for the DS/EN method with an initial bow imperfection is derived. The limit state function is based on Eq. (A.1).

$$\frac{N_{Ed}}{\chi A f_{yk}} + k_{zz} \frac{M_{Ed}}{W_{pl} f_{yk}} = 1 \quad (\text{A.1})$$

where

$$M_{Ed} = N_{Ed} u \quad (\text{A.2})$$

$$k_{zz} = C_{mz} (1 + (2\lambda - 0.6)n) \quad (\text{A.3})$$

$$n = \frac{N_{Ed}}{\chi N_{Rd}} \quad (\text{A.4})$$

$$N_{Rd} = f_{yk} A \quad (\text{A.5})$$

When solving Eq. (7.12) two solutions are given with Eq. (A.6) and (A.7).

$$N_{Ed} = -\frac{1}{C_{mz} u (10\lambda - 3)} (0.5(5A\chi C_{mz} u - \sqrt{25A\chi^2 C_{mz}^2 u^2 + 200AW_{Pl}\chi C_{mz}\lambda u - 10AW_{Pl}\chi C_{mz} u + 25W_{Pl}^2 + 5W_{Pl}) f_{yk}) \quad (\text{A.6})$$

$$N_{Ed} = -\frac{1}{C_{mz} u (10\lambda - 3)} (0.5(5A\chi C_{mz} u + \sqrt{25A\chi^2 C_{mz}^2 u^2 + 200AW_{Pl}\chi C_{mz}\lambda u - 10AW_{Pl}\chi C_{mz} u + 25W_{Pl}^2 + 5W_{Pl}) f_{yk}) \quad (\text{A.7})$$

As Eq.(A.7) yields a negative result, this expression is discarded. The definition of the limit state function is therefore based on Eq.(A.6).

The load S is defined with Eq. (A.8).

$$S = (1 - \zeta) G_{dead} + \zeta Q_{snow} \quad (\text{A.8})$$

The limit state function are defined with Eq. (A.9).

$$g = z R x_r - S \quad (\text{A.9})$$

By inserting Eq. (A.6) and (A.8) the limit state function is defined with Eq. (A.10).

$$g = -\frac{1}{C_{mz} u (10\lambda - 3)} (0.5z(5A\chi C_{mz} u - \sqrt{25A\chi^2 C_{mz}^2 u^2 + 200AW_{Pl}\chi C_{mz}\lambda u - 10AW_{Pl}\chi C_{mz} u + 25W_{Pl}^2 + 5W_{Pl}) f_{yk} x_r) - (1 - \zeta) G_{dead} - \zeta Q_{snow} \quad (\text{A.10})$$